Growing uncertainty in projected spring onset variability in the Northern Hemisphere

Xiaolu Li[1], Toby Ault[1], Colin P Evans[1], Flavio Lehner[2], Carlos M. Carrillo[1], Alison Donnelly[3], T.M. Crimmins[4], amanda gallinat[5], and Mark D Schwartz[6]

[1]Cornell University
[2]Department of Earth and Atmospheric Sciences, Cornell University
[3]The University of Wisconsin-Milwaukee
[4]4USA National Phenology Network, School of Natural Resources and the Environment, University of Arizona,
[5]Unknown
[6]University of Wisconsin-Milwaukee

November 24, 2022

Abstract

Plant phenology regulates the carbon cycle and land-atmosphere coupling. Currently, climate models often disagree with observations on the seasonal cycle of vegetation growth, partially due to how spring onset is measured and simulated. Here we use both thermal and leaf area index (LAI) based indicators to characterize spring onset in CMIP6 models. Although the historical timing varies considerably across models, most agree that spring has advanced in recent decades and will continue to arrive earlier with future warming. Across the Northern Hemisphere for the periods 1950-2014, 1981-2014, and 2015-2099, thermal-based indicators estimate spring advances of -0.7±0.2, -1.4±0.4, and -2.4±0.7 days/decade, while LAI-based indicators estimate -0.4±0.3, -0.1±0.3, and -1±1.1 days/decade. Thereby, LAI-based indicators exhibit later spring and weaker trends toward earlier onset, leading to index-related uncertainty being as large or larger than model uncertainty for a given index. Reconciling index-related discrepancies is therefore critical for understanding future changes in spring onset.

Geophysical Research Letters

Supporting Information for

Growing uncertainty in projected spring onset variability in the Northern Hemisphere

Xiaolu Li[1], Toby Ault[1], Colin P. Evans[1], Flavio Lehner[1,2], Carlos M. Carrillo[1], Alison Donnelly[3], Theresa Crimmins[4], Amanda S. Gallinat[3], Mark D. Schwartz[3]

1] Department of Earth and Atmospheric Sciences, Cornell University, Ithaca, NY 14850, USA

2] Climate and Global Dynamics Laboratory, National Center for Atmospheric Research, Boulder, CO 80302, USA

3] Department of Geography, University of Wisconsin-Milwaukee, Milwaukee, WI 53201, USA

4] USA National Phenology Network, School of Natural Resources and the Environment, University of Arizona, Tucson, AZ 85721, USA

Contents of this file

Text S1 to S2 Figures S1 to S13 Tables S1 to S2

Introduction

The supplementary text includes additional details of the Coupled Model Intercomparison Project Phase 6 (CMIP6) outputs we used to calculate the spring onset indicators and the observational and remote-sensing derived datasets we adopted to validate the model outputs.

Text S1 Additional information on the CMIP6 models

We obtained daily maximum and minimum surface air temperature (tasmax and tasmin) and leaf area index (LAI) from participating models in the CMIP6 ensemble (https://esgf-node.llnl.gov/search/cmip6/) from both historical simulations from the core Diagnostic, Evaluation and Characterization of Klima (DECK) experiments and SSP5-8.5 scenario simulations from the Scenario Model Intercomparison Project. The historical simulations run from 1850-2014 and are forced with estimates of natural (e.g., volcanic eruptions, solar variability) and anthropogenic (e.g., greenhouse gas emissions, land-use change) climate forcing. The Shared Socioeconomic Pathways (SSPs) present alternative scenarios of future emissions and land-use changes estimated using integrated assessment models and run from 2015–2100 except for long-term extensions. Table S1 lists model information for all 26 CMIP6 models used, and Table S2 describes the phenology schemes of the models with daily LAI and prognostic phenology. Although we calculated SI-x for up to 30 members for models with multiple ensemble members, we only included the 1st member (listed in Table S1) in the multi-model analysis (Hagedorn et al., 2005; Lehner et al., 2020). Although members of the same model could experience disagreements on the spring onset trends even at a hemispheric scale due to internal climate variability (Figure S7), they agree on mean spring onset timing (Figure S2) and experience a smaller spread of trend variability at a longer timescale (i.e., compared to the 1979-2014 means in Figure S1, the spread of mean trends of the members from the same model is smaller over the 1950-2014 period).

When phenology is simulated prognostically through biogeochemical processes, LSMs calculate LAI based on carbon allocation to the leaf carbon pool (e.g. Krinner et al., 2005; Lawrence et al., 2019). The start and end of the growing season can be simulated explicitly and determined by environmental factors such as surface air temperature, soil moisture, and daylength (Krinner et al., 2005; Lawrence et al., 2019; Sitch et al., 2003). For instance, in the Community Land Model version 4.5 (CLM4.5, the land surface model used in CMCC-ESM2) and the Organising Carbon and Hydrology In Dynamic Ecosystems v2.0 (ORCHIDEE v2.0, the land surface model of IPSL-CM6A-LR), for unmanaged deciduous ecosystems, onset is explicitly regulated by a growing degree day (GDD) threshold for seasonal deciduous plants (plus chilling in ORCHIDEE) whereas combined thermal, chilling and water stress criteria are required for moisture-limited plants (Botta et al., 2000; Krinner et al., 2005; Lawrence et al., 2019; White et al., 1997). Alternatively, phenology can be modeled implicitly, where onset and offset of the growing season are not explicitly regulated and LAI follows variations in leaf biomass (e.g., as in Surfex 8.0c, the LSM of CNRM-ESM2-1; Hamdi et al., 2014). In addition, some models prescribe phenology to simulate the carbon cycle (e.g., as in CABLE2.4, the LSM of ACCESS-ESM1-5; Law et al., 2017; see Tables S1-S2 for more details).

Text S2 Observational and remote-sensing derived dataset

We adopted gridded daily temperature from both the Berkeley Earth Surface Temperature Gridded Land Daily Temperature dataset (hereafter Berkeley Earth, http://berkeleyearth.org/data/) and the Climate Prediction Center Global Daily Temperature (hereafter CPC, https://psl.noaa.gov/data/gridded/data.cpc.globaltemp.html). The Berkeley Earth Gridded Land Daily Temperature dataset includes daily maximum and minimum temperature at a 1° × 1° latitude-longitude grid from 1880 to 2021. Uncertainties in gridded temperature records at a hemispheric scale are greater prior to 1950 due to decreasing data availability and spatial coverage of weather stations, so we calculated thermal-based indices from 1950 to 2014 to be consistent with the historical simulations. The CPC temperatures are 0.5° × 0.5° latitude-longitude resolution daily data calculated using the CPC archive of Global Telecommunication System daily reports and the Shepard algorithm. CPC covers 1979-2021 and we used 1979-2014 to compare against historical simulations.

To assess simulated LAI amplitude and seasonality, we also adopted the Global LAnd Surface Satellite LAI. This product provides eight-day composites of LAI, based on the Advanced Very High Resolution Radiometer (AVHRR) reflectance data. We obtained the 0.5° x 0.5° dataset and aggregated the raw GLASS LAI to a 1° x 1° latitude/longitude grid by averaging the four GLASS grid points in each model grid. We then fitted a smoothing spline to the time series of each grid point for each year and used it to interpolate the 8-day data to daily resolution. Finally, we calculated the day-of-year (DOY) time series of spring onset as indicated by different LAI thresholds.

Supplementary Figures

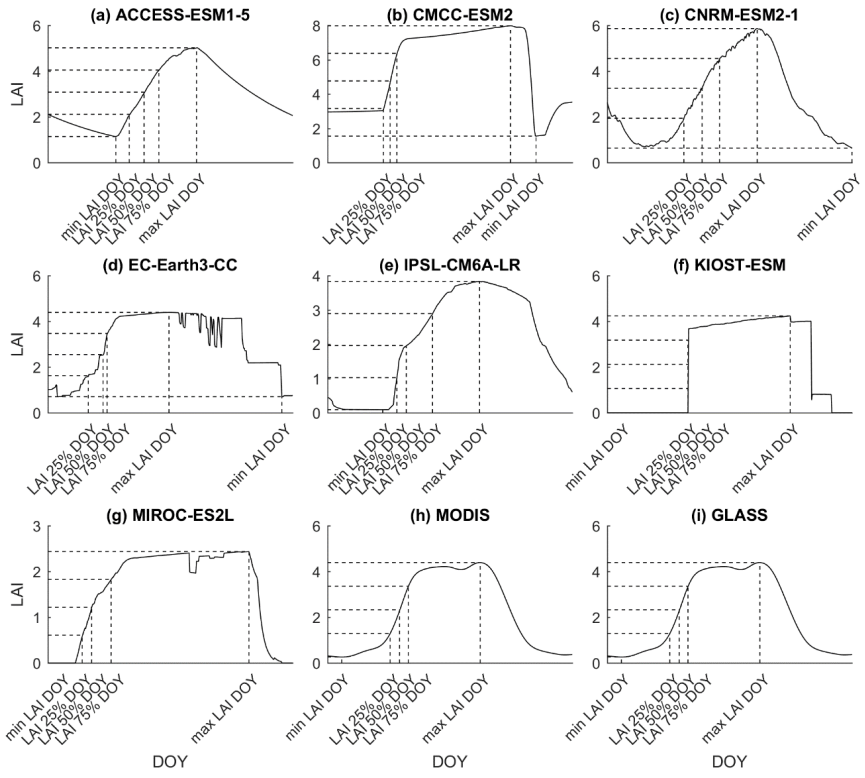

Figure S1 Illustrative diagram showing how the LAI threshold-based DOY indices are computed from the

simulated LAIs (panels a-g), MODIS LAI (h), and GLASS LAI (i). The diagram presents daily LAI in the year 2010, the LAI thresholds, and LAI threshold-based day of year (DOY) at 38.5°N, 82.5°W. We define the annual dynamical range of LAI as the difference between the annual minimum (min LAI) and maximum LAI (max LAI). We then calculate spring onset indicators based on the day of year LAI passes the 25%, 50%, and 75% thresholds of its annual dynamical range.

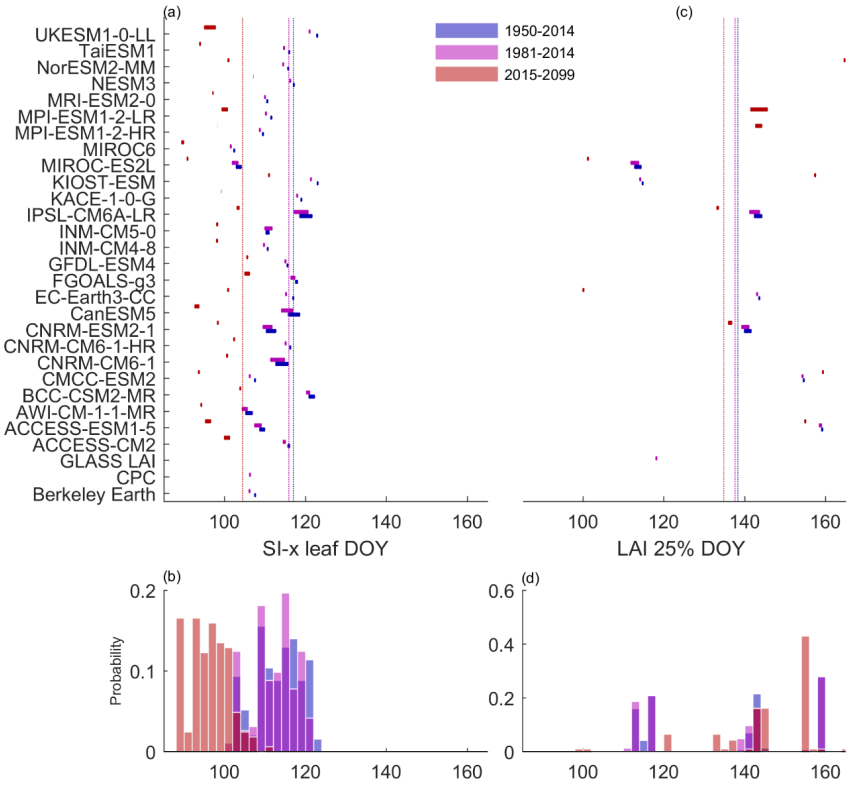

Figure S2 Mean day of year (DOY) of SI-x leaf (left) and LAI25% (right) averaged across the Northern Hemisphere (25°N-85°N) for each model member and the observational datasets. Mean SI-x leaf and LAI25% are calculated over 1950-2014 (blue), 1981-2014 (magenta), and 2015-2099 (orange) periods and weighted by area weight. Ensemble means averaged across the first member of each model (26 models for SI-x leaf and 7 models for LAI25%) are plotted vertically for comparison.

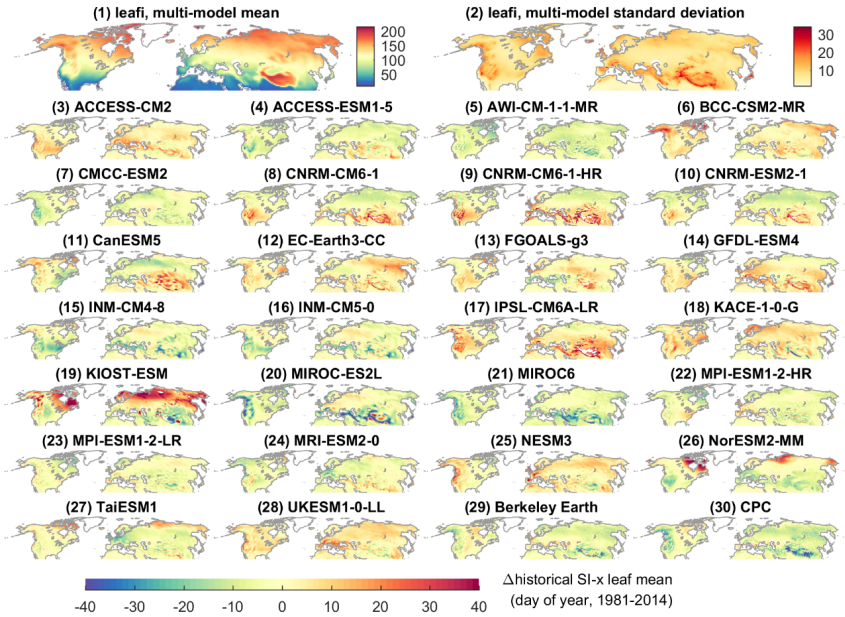

Figure S3 Ensemble mean and standard deviation of the SI-x leaf index and departure of each model and observations from the ensemble mean. Panels (1) and (2): mean (1) and standard deviation (2) of spring onset timing as indicated by SI-x leaf across the first member of the 26 CMIP6 models during 1981-2014 in the historical simulations. Panels (3-28): differences between each model 1981-2014 mean SI-x leaf and the ensemble mean. Panels (29-30): differences between the two observation-based mean first leaf and the model ensemble mean.

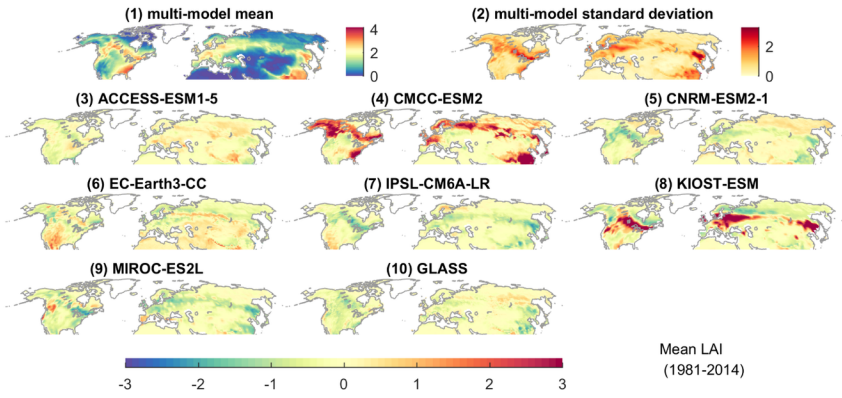

Figure S4 Ensemble mean and standard deviation of the leaf area index (LAI) and departure of each model and the Global LAnd Surface Satellite (GLASS) LAI from the ensemble mean. Panels (1) and (2): mean (1) and standard deviation (2) of mean LAI across the first member of the seven CMIP6 models during the 1981-2014 historical period. Panels (3-9): differences between each model and the ensemble mean LAI. Panels (10): differences between the GLASS LAI and the model ensemble mean.

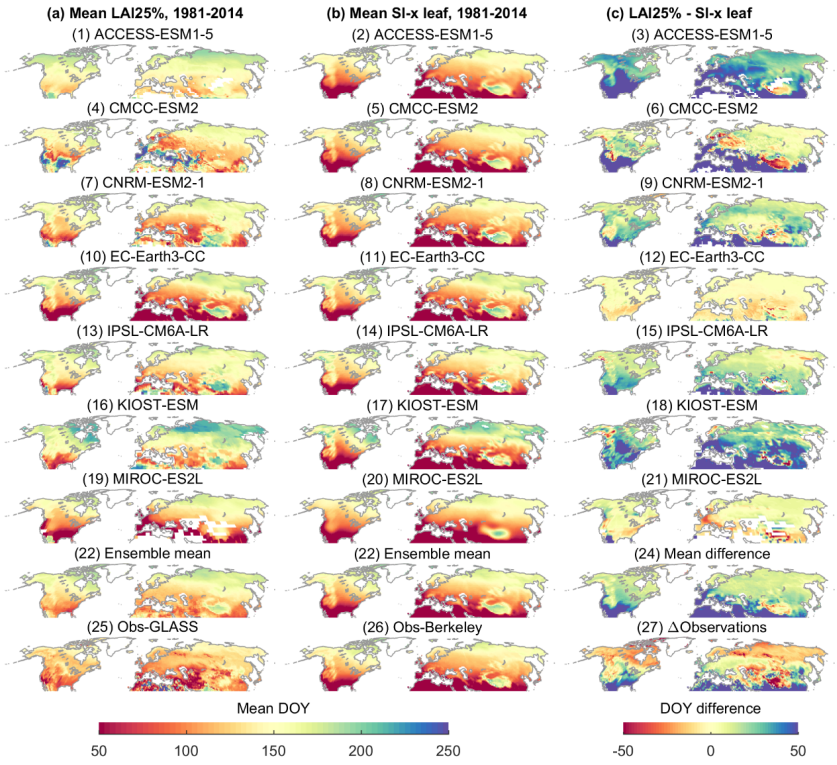

Figure S5 Mean day of year (DOY) of mean LAI25% DOY (a), mean SI-x leaf DOY (b), and the difference between the two (c) during the 1981-2014 historical period for the seven models with both daily temperature and LAI output (1-7th rows), the ensemble mean (8th row), and observations (bottom row).

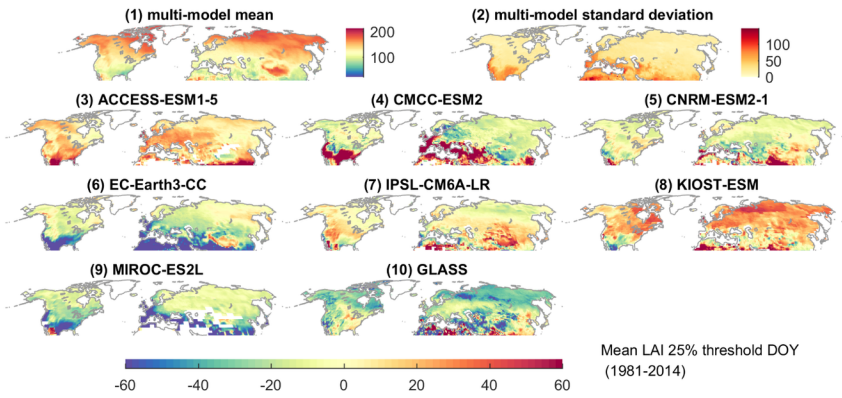

Figure S6 Ensemble mean and standard deviation of the LAI 25% threshold DOY (LAI25%) and departure of each model and the GLASS LAI from the ensemble mean during 1981-2014. Panels (1) and (2): mean (1) and standard deviation (2) of LAI25% of the seven CMIP6 models during the 1981-2014 historical period. Panels (3-9): differences between each model and the ensemble mean DOY. Panels (10): differences between Obs-GLASS-LAI25% and the model ensemble mean.

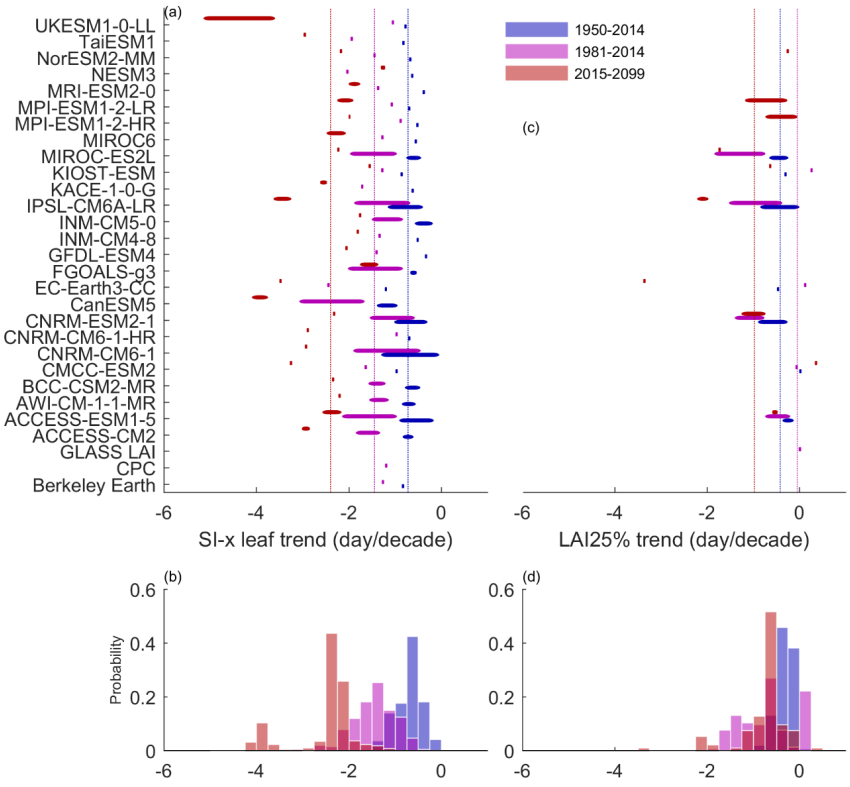

Figure S7 Mean trend of the SI-x leaf (left) and LAI25% (right) averaged across the Northern Hemisphere (25°N-85°N) for each model member and the observational datasets. Mean SI-x leaf and LAI25% trends are calculated over 1950-2014 (blue), 1981-2014 (magenta), and 2015-2099 (orange) periods and weighted by area weight. Ensemble means averaged across the first member of each model (26 models for SI-x leaf and 7 models for LAI25%) are plotted vertically for comparison.

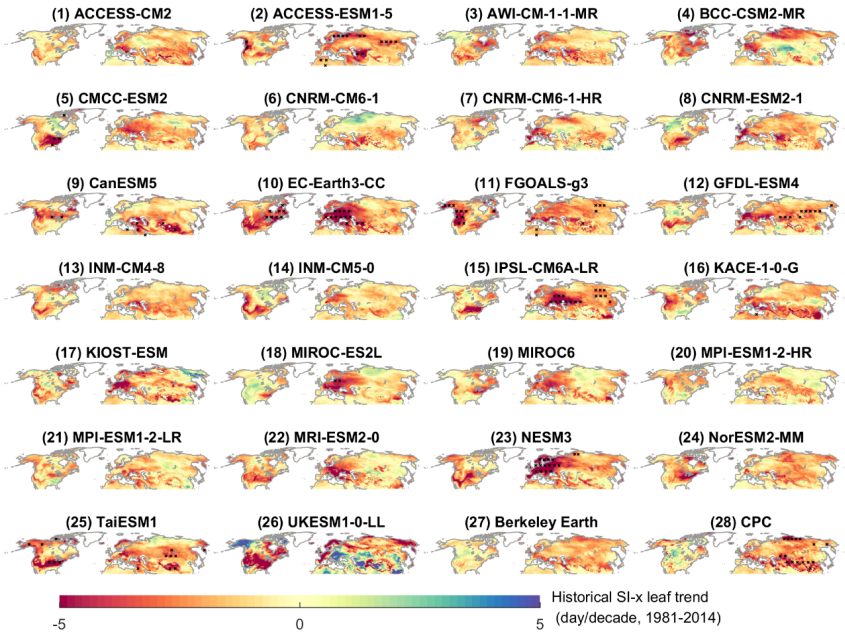

Figure S8 Maps showing SI-x leaf trends over the historical period (1981-2014). Grid cell with a significant trend after adjusting for false positive is marked with a black "x". Panel (1-26) SI-x leaf trend of the 26 CMIP6 models. Panels (27-28): Trend of observation-based first leaf estimates.

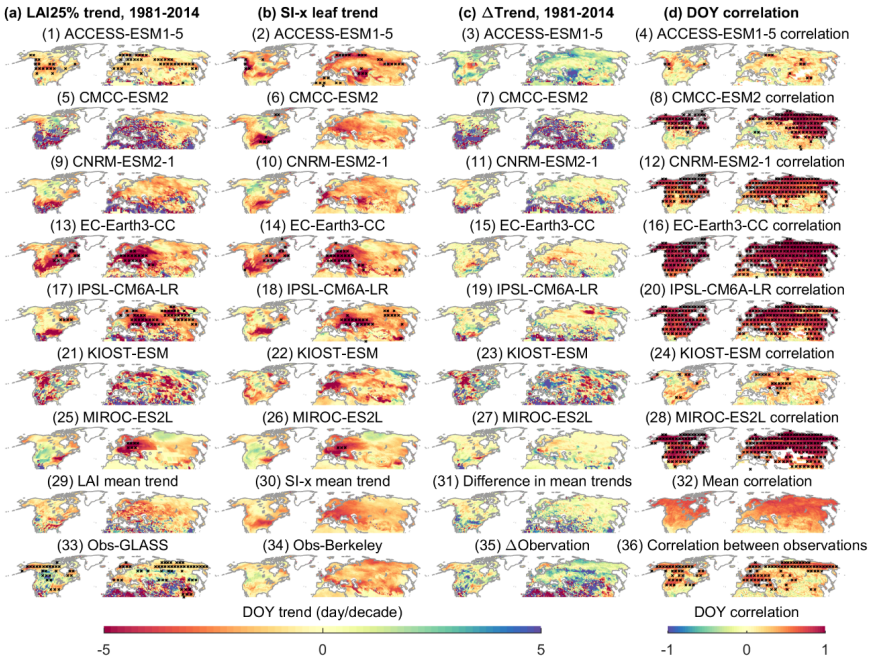

Figure S9 Trends of LAI25% (a), SI-x leaf (b), the difference between the two (c), and correlation between the detrended DOYs (d) during the 1981-2014 historical period for the seven models with both daily temperature and LAI output (1-7th rows), the ensemble mean (8th row), and observations (last row). Grid cell with a significant trend/correlation ($p<0.05$) after adjusting for false positive is marked with a black "x".

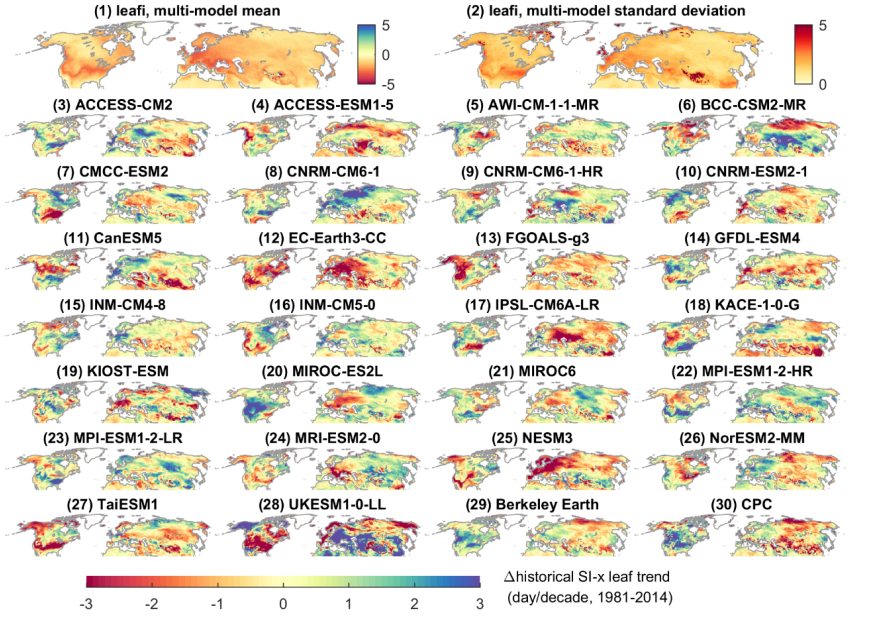

Figure S10 Ensemble mean and standard deviation of the SI-x leaf trend and departure of each model from the ensemble mean. Panels (1) and (2): mean (1) and standard deviation (2) of trends in spring onset timing as indicated by SI-x leaf across the first member of the 26 CMIP6 models during the 1981-2014 historical period. Panels (3-28): differences between each model trend and the ensemble mean. Panels (29-30): differences between the two observation-based first leaf trends and the model ensemble mean.

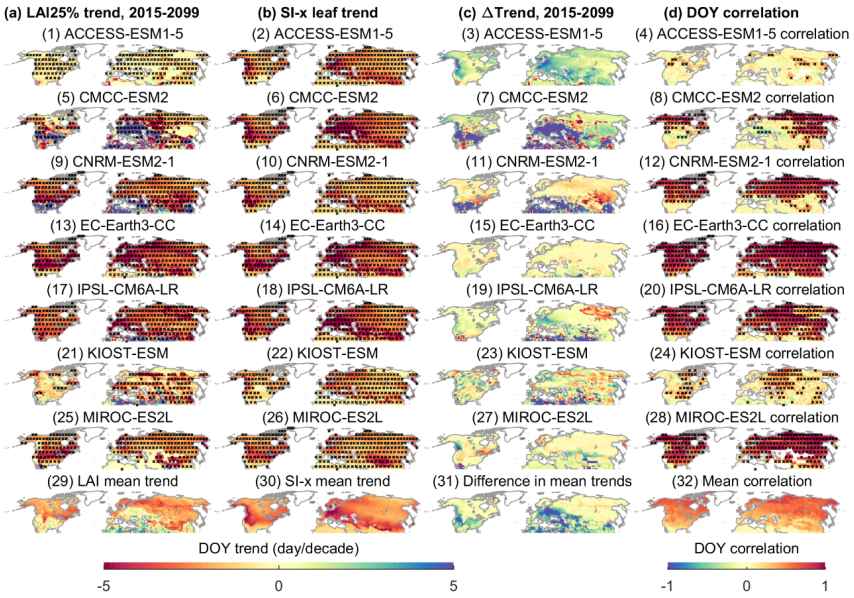

Figure S11 Trends of LAI25% (a), SI-x leaf (b), difference between the two (c), and correlation between the detrended DOYs (d) during 2015-2099 under the SSP585 scenario for the seven models with both daily temperature and LAI output (1-7th rows) and the ensemble mean (8th row). Grid cell with a significant trend/correlation ($p<0.05$) after adjusting for false positive is marked with a black "x".

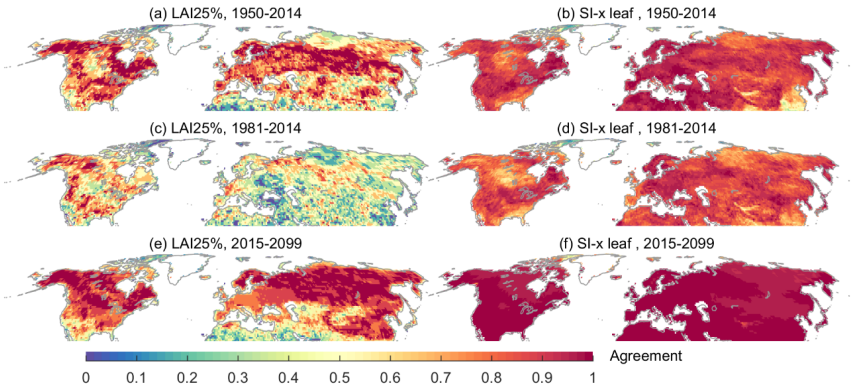

Figure S12 Proportion of models with an earlier spring onset (negative trend) of LAI25% (left) and SI-x leaf (right) during different time periods. LAI25% trends are calculated based on the seven models and SI-x trends are averaged across all 26 models.

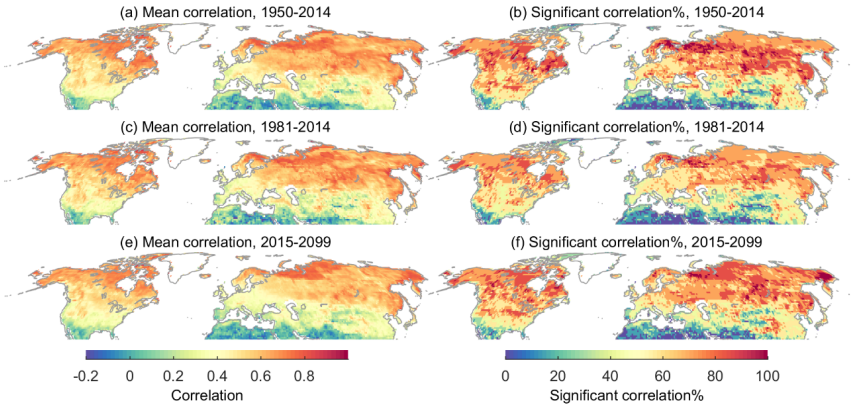

Figure S13 Ensemble mean correlation between SI-x leaf and LAI25% and proportion of models with a significant positive correlation ($p<0.05$) during different time periods. Mean correlations (left column) are averaged over correlations of the seven CMIP6 models with both daily temperature and LAI available. Larger proportion of models (right column) means more models exhibit a significant positive correlation ($p<0.05$) between the thermal- and LAI-based spring onset indicators.

Supplementary Tables

Table S1 Information on the 26 CMIP6 models

Models	Run/member used in the analysis	Horizontal resolution (latxlon)	Atmospheric model	Oce
ACCESS-CM2	r1i1p1f1	1.88 x 1.25	MetUM-HadGEM3-GA7.1	AC
ACCESS-ESM1-5	r1i1p1f1	1.88 x 1.24	HadGAM2	AC
AWI-CM-1-1-MR	r1i1p1f1	0.94 x 0.94	ECHAM6.3.04p1	FES
BCC-CSM2-MR	r1i1p1f1	1.13 x 1.13	BCC_AGCM3_MR	MC
CMCC-ESM2	r1i1p1f1	1.25 x 0.94	CAM5.3	NE
CNRM-CM6-1	r1i1p1f2	1.41 x 1.41	Arpege 6.3	
CNRM-CM6-1-HR	r1i1p1f2	0.50 x 0.50	Arpege 6.4	
CNRM-ESM2-1	r1i1p1f2	1.41 x 1.41	Arpege 6.5	Ner
CanESM5	r1i1p1f1	2.81 x 2.81	CanAM5	NE
EC-Earth3-CC	r1i1p1f1	0.70 x 0.70	IFS cy36r4	NE
FGOALS-g3	r1i1p1f1	2.00 x 2.25	GAMIL2	LIC
GFDL-ESM4	r1i1p1f1	1.25 x 2.00	GFDL-AM4.1	GF
INM-CM4-8	r1i1p1f1	2.00 x 1.50	INM-AM4-8	INM
INM-CM5-0	r1i1p1f1	2.00 x 1.50	INM-AM5-0	INM
IPSL-CM6A-LR	r1i1p1f1	2.50 x 1.26	LMDZ (NPv6)	NE
KACE-1-0-G	r1i1p1f1	1.88 x 2.50	MetUM-HadGEM3-GA7.1	MC
KIOST-ESM	r1i1p1f1	1.88 x 1.88	GFDL-AM2.0	GF
MIROC-ES2L	r1i1000p1f2	2.81 x 2.81	CCSR AGCM	CO
MIROC6	r1i1p1f1	1.41 x 2.81	CCSR AGCM	CO
MPI-ESM1-2-HR	r1i1p1f1	0.94 x 1.88	ECHAM6.3	MP
MPI-ESM1-2-LR	r1i1p1f1	1.88 x 3.75	ECHAM6.3	MP
MRI-ESM2-0	r1i1p1f1	1.13 x 2.25	MRI-AGCM3.5	MR
NESM3	r1i1p1f1	1.88 x 3.75	ECHAM v6.3	NE
NorESM2-MM	r1i1p1f1	1.25 x 1.88	CAM-OSLO (CAM6-Nor)	MI
TaiESM1	r1i1p1f1	1.25 x 0.94	TaiAM1	PO
UKESM1-0-LL	r1i1p1f2	1.88 x 2.50	MetUM-HadGEM3-GA7.1	NE

Table S2 Information of spring onset triggers and/or leaf phenology in the land surface models in the seven CMIP6 models with a prognostic carbon cycle and daily LAI outputs

Models	Land model	Phenology/Spring onset
ACCESS-ESM1-5	CABLE2.4	The phenology phase is prescribed by latitude and vegetation type and based on remote sensing data.

Models	Land model	Phenology/Spring onset
CMCC-ESM2	CLM4.5 BGC	Spring onset of deciduous plant functional types (PFT) depends on environmental factors: growing degree day (GDD) accumulation for seasonal deciduous PFTs; GDD, chilling, and soil moisture accumulation for stress deciduous PFTs (GDD exceeds a critical threshold if chilling exceeds 15 days; soil water potential exceeds the critical threshold for more than 15 days; daylength is over 6 hours).
CNRM-ESM2-1	Surfex 8.0c	Phenology is modeled implicitly: LAI follows the variations of leaf biomass.
EC-Earth3-CC	HTESSEL and LPJ-GUESS v4	Spring onset is based on a simple temperature model (TAS>5); grasses can shed their leaves under conditions of severe water stress.
IPSL-CM6A-LR	ORCHIDEE (v2.0)	Spring onset of deciduous PFTs depends on environmental factors: GDD and chilling requirements for cold deciduous PFTs while GDD, chilling, and soil water criteria for stress deciduous PFTs.
KIOST-ESM	Land Model version 3.0 (LM3.0)	Phenology is governed by monthly environmental triggers: onset is triggered when mean monthly canopy air temperature is above 10°C and the mean monthly plant-available soil water in the root zone is more than 10% of its maximum possible value.
MIROC-ES2L	MATSIRO6.0+VISIT-e ver.1.0	Leaf onset is based on cumulative temperature (no explicit water effect).

Hosted file

essoar.10512515.1.docx available at https://authorea.com/users/542218/articles/604950-growing-uncertainty-in-projected-spring-onset-variability-in-the-northern-hemisphere

Authors: Xiaolu Li[1], Toby Ault[1], Colin P. Evans[1], Flavio Lehner[1, 2], Carlos M. Carrillo[1], Alison Donnelly[3], Theresa Crimmins[4], Amanda S. Gallinat[3], Mark D. Schwartz[3]

[1] Department of Earth and Atmospheric Sciences, Cornell University, Ithaca, NY 14850, USA

[2] Climate and Global Dynamics Laboratory, National Center for Atmospheric Research, Boulder, CO 80302, USA

[3] Department of Geography, University of Wisconsin-Milwaukee, Milwaukee, WI 53201, USA

[4] USA National Phenology Network, School of Natural Resources and the Environment, University of Arizona, Tucson, AZ 85721, USA

Corresponding author: Xiaolu Li (xl552@cornell.edu)

Key Points:

- Divergence between thermal- and growth-based spring onset indicators grows with time as global temperatures increase.
- Thermal-based indicators estimate spring advances of -0.7, -1.4, and -2.4 days/decade in 1950-2014, 1981-2014, and 2015-2099.
- Vegetation growth-based indicators exhibit later spring, weaker trends toward earlier spring onset, and larger disagreements among models.

Abstract

Plant phenology regulates the carbon cycle and land-atmosphere coupling. Currently, climate models often disagree with observations on the seasonal cycle of vegetation growth, partially due to how spring onset is measured and simulated. Here we use both thermal and leaf area index (LAI) based indicators to characterize spring onset in CMIP6 models. Although the historical timing varies considerably across models, most agree that spring has advanced in recent decades and will continue to arrive earlier with future warming. Across the Northern Hemisphere for the periods 1950-2014, 1981-2014, and 2015-2099, thermal-based indicators estimate spring advances of -0.7±0.2, -1.4±0.4, and -2.4±0.7 days/decade, while LAI-based indicators estimate -0.4±0.3, -0.1±0.3, and -1±1.1 days/decade. Thereby, LAI-based indicators exhibit later spring and weaker trends toward earlier onset, leading to index-related uncertainty being as large or larger than model uncertainty for a given index. Reconciling index-related discrepancies is therefore critical for understanding future changes in spring onset.

Plain Language Summary

The timing of spring onset as indicated by green-up affects plants, bird and insect populations, rivers, and agriculture. However, state-of-the-art land surface

models disagree with satellite-derived records on the seasonal cycles of vegetation growth, making it difficult to accurately predict green-up, its response to climate, and the ecological consequences. Here we calculate two sets of spring onset indicators using climate model outputs to characterize spring onset variations and trends in the recent past and future. We find spring has been advancing in recent decades and will continue to arrive earlier with future warming. Thermal-based indicators show that spring onset advances by -0.7, -1.4, and -2.4 days/decade in the Northern Hemisphere during 1950-2014, 1981-2014, and 2015-2099, respectively. This result suggests that spring onset today is on average four days earlier than spring onset 30 years ago and this rate will nearly double in the future. However, compared to meteorological-based indicators, vegetation growth-based indicators exhibit later spring and weaker trends toward earlier onset. Therefore, how we define and measure spring onset as well as the models we use to predict changes in the environmental factors influence future changes in spring onset.

1 Introduction

Understanding spring plant phenology is essential as it modulates ecosystem functions, the terrestrial carbon cycle, and land-atmosphere coupling (Morisette et al., 2009; Renner & Zohner, 2018; Richardson et al., 2013). In temperate and boreal regions, plant phenology modifies the terrestrial carbon cycle by governing growing season onset and duration (Morisette et al., 2009; Richardson et al., 2009, 2010). In addition, plant phenophase changes regulate land-atmosphere energy and momentum exchanges (Richardson et al., 2013; Schwartz, 1992), and therefore influence land-atmosphere coupling strength, as demonstrated by both observations (Berg et al., 2016; Findell et al., 2015; Green et al., 2017) and model experiments (Guillevic et al., 2002; Levis & Bonan, 2004; Lorenz et al., 2013; Puma et al., 2013; Xu et al., 2020). Human-induced changes in temperature and precipitation will likely modify plant phenology in the future, which in turn will affect carbon sequestration and energy exchanges between the biosphere and the atmosphere (Morisette et al., 2009; Richardson et al., 2013). Therefore, understanding and evaluating phenology variabilities at high temporal resolution is critical for accurate climate projections.

Two approaches have been widely adopted to simulate how spring onset responds to climate variability and long-term warming. Firstly, indicator models of the start of spring, like the spring indices, have been extensively used to characterize trends and variability of spring onset and identify the influence of abiotic factors (Ault, Zurita-Milla, et al., 2015; Chuine et al., 1998; Jolly et al., 2005; Schwartz et al., 2006). Because these indicator models are offline (i.e., not coupled to meteorological variables) and focus on specific growth stages (e.g., leaf out, blooming) instead of carbon allocation during vegetation growth, their computational cost is much less than in the second approach -- land surface models (LSM), and are more complex and finely tuned to specific species or plant functional types (PFT) than phenology schemes in LSMs (Krinner et al., 2005; Milly et al., 2014; Sitch et al., 2003). In addition, as they only rely

on meteorological variables and can be applied and compared uniformly across models, indicator models have been adopted to estimate projected spring onset variability (Allstadt et al., 2015; Zhu et al., 2019). However, as temperature increases, the relative importance of meteorological and biotic factors in regulating spring onset timing may change (Flynn & Wolkovich, 2018; Fu et al., 2015; Laube et al., 2014; Park et al., 2021; Parmesan, 2007; Renner & Zohner, 2018), increasing uncertainty in how natural and managed ecosystems will adapt to climate change.

Simulating plant phenology using LSMs is another approach for predicting phenology changes in the future and their influences on the Earth system. State-of-the-art LSMs adopt environmental conditions (i.e., temperature, soil moisture, etc.) to simulate plant phenology prognostically (e.g. Krinner et al., 2005; Oleson et al., 2013), but large discrepancies are present in both the amplitude of leaf area index (LAI) and land surface phenology simulated by climate models and derived from satellite imagery (Mahowald et al., 2016; Park & Jeong, 2021; Peano et al., 2019; Richardson et al., 2012; Song et al., 2021), potentially inducing large influences on land surface states including surface temperature(Lorenz et al., 2013; Xu et al., 2020). In addition, although plant phenology is often simulated at a daily or higher temporal resolution (Krinner et al., 2005; Oleson et al., 2013; Sitch et al., 2003), model output is often documented at a coarser resolution and therefore most evaluations are based on monthly averages, adding to uncertainties and undermining the trends (Park & Jeong, 2021; Peano et al., 2019; Song et al., 2021). Meanwhile, not all climate models simulate plant phenology and the carbon cycle prognostically, posing additional uncertainties in future projections of land-atmosphere interactions and terrestrial carbon cycles.

Here we adopt both a suite of thermal-based indicators -- the extended spring indices models (SI-x; Schwartz, 1997; Schwartz et al., 2006; Schwartz & Reiter, 2000) -- and plant phenology from the Coupled Model Intercomparison Project Phase 6 (CMIP6; Eyring et al., 2016) to characterize the timing and variation of spring onset in CMIP6 simulations. While both indicators are widely used to infer changes in seasonal transitions and plant phenology, they are yet to be compared in the instrumental period and future projections. We aim to assess the historical and projected variabilities and uncertainties of spring onset timing in the Northern Hemisphere, which play an important role in modulating both the carbon cycle and land-atmosphere interactions.

2 Data and Methods

2.1 CMIP6 models

We obtained daily maximum and minimum surface air temperature and leaf area index (LAI) from participating models in the CMIP6 ensemble from both historical and SSP5-8.5 scenario simulations (Eyring et al., 2016; O'Neill et al., 2016; see Text S1 for details). To estimate changes in the timing of spring onset under the most pessimistic conditions, we adopted the SSP5-8.5 scenario (hereafter SSP585) which estimates a +8.5 W/m^2 increase in radiative forcing

and represents a high-emission, high-end forcing pathway (O'Neill et al., 2016). We used 1950-2099 daily maximum and minimum surface air temperature from all 26 models with both historical and SSP585 daily temperature data available (Table S1). Seven models also have prognostic carbon cycle and daily LAI available (Table S2 and Text S1). For models with leap years, we removed temperature and LAI data for Feb 29th to form a consistent comparison among models. We used bilinear interpolation to adapt all model outputs to a $1° \times 1°$ latitude-longitude resolution.

2.2 The extended spring indices model

The extended spring indices (SI-x) and their predecessors, the original SI were developed from historical records of lilac and honeysuckle phenology, and have been extensively used as proxies for certain groups of species, as well as to assess the impact of abiotic changes on spring onset (Ault, Schwartz, et al., 2015; Gerst et al., 2020; Schwartz, 1997; Schwartz et al., 2006, 2013; Schwartz & Marotz, 1986; Schwartz & Reiter, 2000). SI-x uses daily minimum and maximum temperatures and latitude to estimate the timing of spring foliage (first leaf, hereafter SI-x leaf) and blooming (first bloom) for plants with temperature-responsive phenology. It has also been extended to warmer locations that may not meet the chill requirements of the original SI (Schwartz et al., 2013). Here we calculated SI-x leaf for all 26 models at $1° \times 1°$ resolution from 1950-2099 and the observations from 1950-2014 (Berkeley Earth, see Text S2) and 1979-2014 (CPC, Text S2).

2.3 LAI threshold-based DOY

We also calculated spring onset indicators based on the day of year LAI reaches pre-defined thresholds of its annual dynamical range. The dynamical range of LAI is defined as the difference between minimum (winter) and maximum (summer) LAI each year. We focused on the 25%, 50%, and 75% thresholds of the annual dynamical range of LAI (Figure S1). Using threshold-based indicators reduces the influence of land-use change as well as differences in peak LAI from one year to the next (White et al., 1997). Similar methods have been adopted to determine the start of the growing season from monthly records (Peano et al., 2019; Richardson et al., 2012; Song et al., 2021), and with daily LAI we were able to achieve more precise timing and compare it with DOY records from thermal-based indicator models. We focused on SI-x leaf and LAI25% (i.e., the early spring events) in the analysis as we are interested in the trends and variability of the full possible ranges of spring onset.

2.4 Statistical method

We calculated linear trends of the indices over different time windows and used a one-tailed 5% significance level to evaluate the importance of all analyzed trends. When calculating correlations between the indicators, we first removed the linear trend and then calculated correlation coefficients of the detrended time series. The significance of the trends and correlations have been adjusted for

false discovery by recalculating the significance level to control the expectation of falsely rejected hypotheses (Benjamini & Hochberg, 1995).

3 Results

3.1 Spring onset timing

Spring onset timing has advanced in recent decades in both observations and model simulations and will shift earlier under the SSP585 scenario (Figures 1-3). Over 1950-2014 in the Northern Hemisphere (NH), CMIP6 ensemble mean of 26 models indicates 117.0±6.0 days to first leaf (hereafter CMIP6-leaf), later than SI-x leaf based on Berkeley Earth (hereafter Obs-Berkeley-leaf, 107.3±2.2 days; Figure S2a). These numbers advance by approximately one day during 1981-2014. Over the historical period, the spread of spring onset timing in CMIP6 encompasses the interannual variability of observation-based SI-x (Figure 1a). Under the SSP585 scenario in 2015-2099, CMIP6-leaf advances to 104.5±8.6 days. The largest disagreement of mean onset dates between CMIP6 models is present in Western NA, Northern Russia, and over the Tibetan Plateau during the historical period, and this spatial pattern persists into the SSP585 period (Figures 2hj and S3).

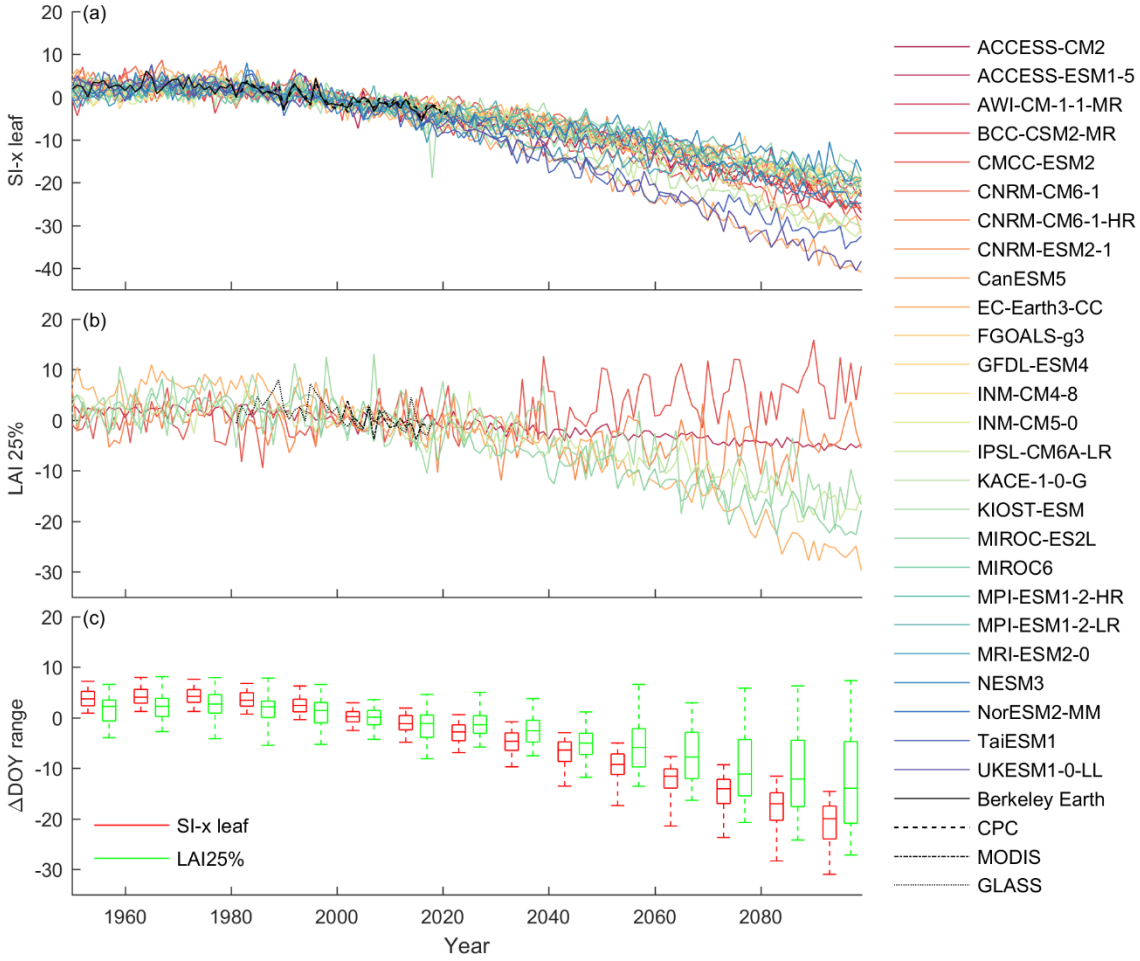

Figure 1 Anomalies in the day of year (DOY) spring onset is predicted. (a): SI-x leaf indices calculated from the 26 CMIP6 models and the Berkeley Earth and CPC gridded daily temperature datasets averaged across the Northern Hemisphere (25°N-85°N) and adjusted for area weight. DOY anomalies are calculated by subtracting the 1981-2010 mean of each model/observation. (b): Day-of-year (DOY) anomalies of the LAI 25% threshold DOYs calculated from the seven CMIP6 models and the GLASS and MODIS LAI averaged across the Northern Hemisphere (25°N-85°N). DOY anomalies are calculated by subtracting the 2001-2014 mean of each model/observation and adjusting for area weight. (c): box plots showing the spread of SI-x leaf and LAI 25% DOYs derived from CMIP6 models during each decade. For each box plot, the centerline denotes the median of the DOYs, box limits show the upper and lower quartiles (25% and 75%), and whiskers indicate the 5% and 95% values.

Models experience considerable differences in simulated plant phenology (Fig-

ure S1), mean LAI values (Figure S4), and mean LAI threshold-based spring onset timing (Figures S1, S2cd, S5a). Compared to GLASS LAI (described in Text S2), ensemble mean overestimates LAI values in Eastern Asia and western Canada and underestimates LAI in Southern Russia (Figure S4). Large disagreements exist among the models in Canada, Northern Europe, and East Asia. These regions continue experiencing large differences among model LAIs in SSP585, along with Eastern US.

The start of spring as indicated by LAI 25% threshold DOYs are much later in the models than in GLASS LAI or those indicated by SI-x leaf (Figures 2, S2, S5). Across the NH, mean LAI 25% DOY based on simulated LAIs (hereafter CMIP6-LAI25%) is 137.7±19.7 during 1981-2014, 20 days later than in GLASS LAI (hereafter Obs-GLASS-LAI25%, 117.9±2.6). CMIP6-LAI25% advances to 134.9±24.4 in 2015-2099 (Figure S2cd). In every period, CMIP6-LAI25% is later than both CMIP6-leaf and Obs-GLASS-LAI25% (Figures 2cf and S2) and exhibits larger inter-model variability than CMIP6-leaf (Figure 1c, 2g-j). The timing also varies considerably across models (Figures 1b, S2cd, S5a). The largest disagreement among models is present south of 40°N while large differences between CMIP6-LAI25% and Obs-GLASS-LAI25% are also present in the Tibetan Plateau, Russia, and Northern Europe. Overall, models estimate later spring onset over high-latitude (north of 55°N) and high-altitude regions (Figure S6).

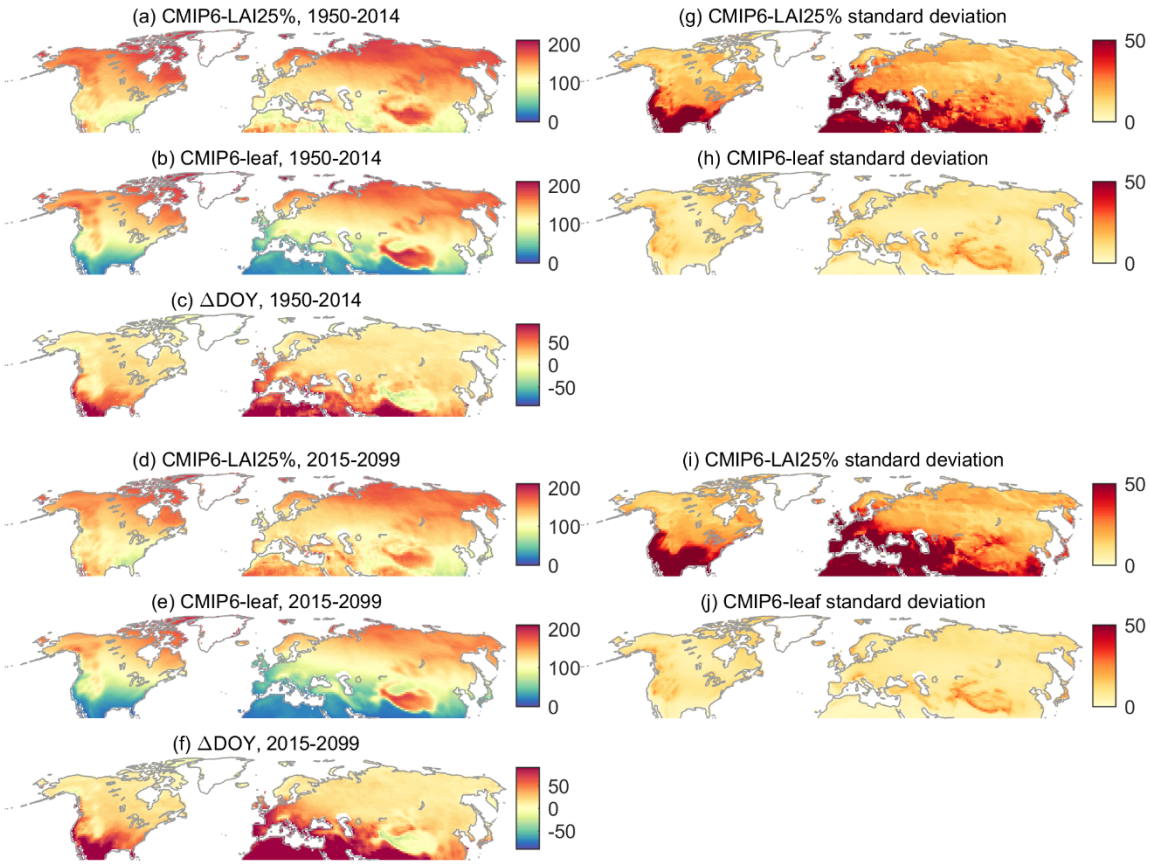

Figure 2 Ensemble mean and standard deviation of the spring onset indicators during the historical and SSP585 periods. (abde): ensemble mean DOY, (cf): difference in mean DOY, and standard deviation of LAI 25% threshold DOY (CMIP6-LAI25%, gi) and SI-x leaf (CMIP6-leaf, hj) during the historical (1950-2014) and SSP585 (2015-2099) periods. CMIP6-LAI25% is calculated based on the seven models and SI-x leaf is averaged across 26 models. Numbers indicate DOYs in (a), (b), (d), and (e), DOY differences (unit: day) in (c) and (f), and DOY standard deviation (unit: day) in (g)-(j).

Differences in mean spring onset timing vary across models and regions (Figures 2 and S5) but increase through time. Difference between CMIP6-leaf and CMIP6-LAI25% is 22 days during 1981-2014 and increases to 30 days under the SSP585 scenario (Figure S2). Across the seven models that provide daily temperature and LAI output, LAI25% is later than SI-x leaf at lower latitudes, though EC-Earth3-CC displays uniformly earlier spring in LAI25% and MIROC-ES2L has earlier LAI indicated spring onset at lower latitudes. Obs-GLASS-LAI25% indicates earlier spring than Obs-Berkeley-leaf in higher latitude and higher elevation regions while model simulations show a reduced advancement in spring

onset (Figure S5c). This pattern persists into the 2015-2099 period with a larger difference between the two sets of indicators. Across the NH, CMIP6-LAI25% exhibits a later spring onset than CMIP6-leaf, with a smaller delay at higher latitudes and higher elevations and a consistent spatial pattern during different simulation periods (Figure 2cf).

3.2 Trends in the start of spring

Long-term trends in the start of spring, as measured by SI-x leaf trends over 1950-2014, exhibit overall agreement between observations and the ensemble mean but vary considerably across models (Figures 3bh, S7ab, S8). During 1950-2014 in the NH, the ensemble mean trend of CMIP6-leaf is -0.72±0.21 day/decade, whereas mean Obs-Berkeley-leaf trend is -0.85 day/decade (Figure S7ab). The magnitude of the trends increases during the more recent period (1981-2014), with CMIP6-leaf mean trends of -1.44±0.4 days/decade, slightly greater than Obs-Berkeley-leaf (-1.28 days/decade) and CPC (Obs-CPC-leaf, -1.21 days/decade). The magnitude of trends increases by ~0.9 day/decade under SSP585. During 2015-2099, CMIP6-leaf exhibits an ensemble mean trend of -2.39±0.71 days/decade. However, the trends vary considerably across models and even among different members of the same model (Figures 3ej, S7ab).

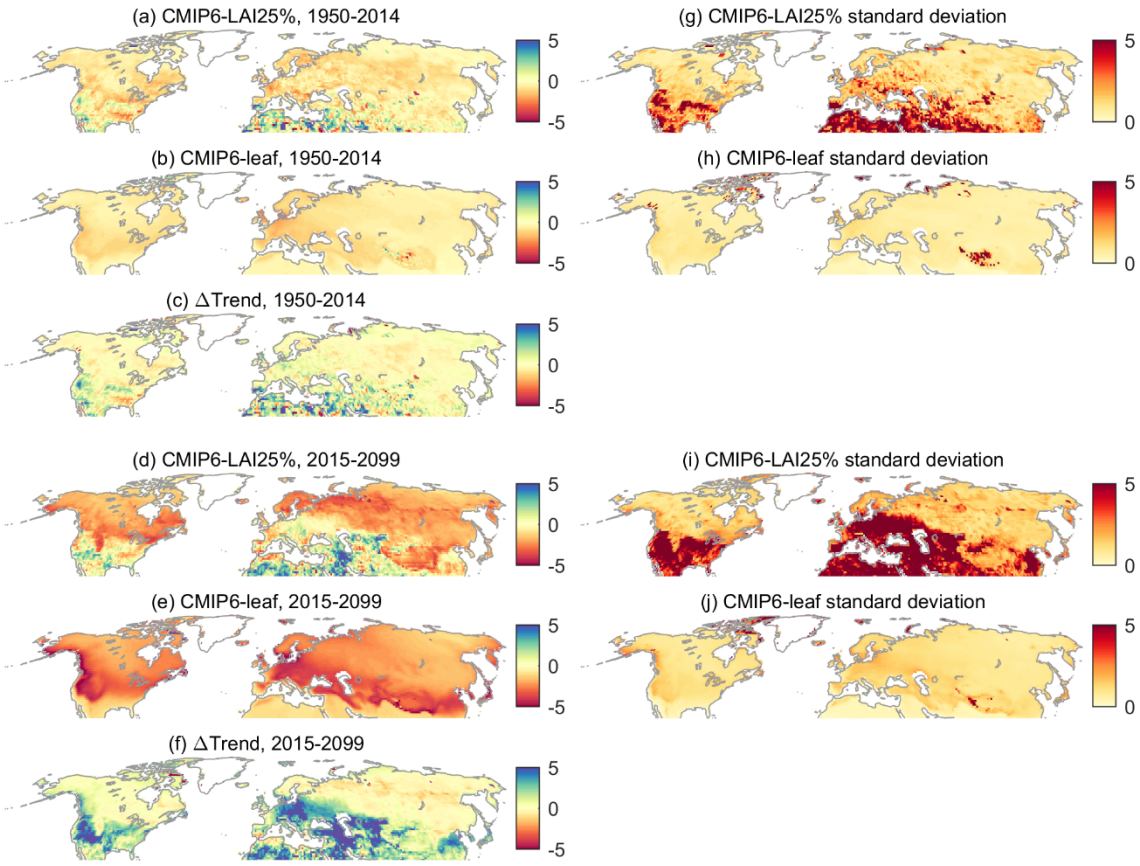

Fig. 3 Ensemble mean and standard deviation of spring onset trends. (abde): ensemble mean trends, (cf): difference in mean trends, and standard deviation between ensemble members of LAI 25% threshold DOY (CMIP6-LAI25%, gi) and SI-x leaf (CMIP6-leaf, hj) during the historical (1950-2014) and SSP585 (2015-2099) periods (unit: day/decade). CMIP6-LAI25% trends are based on the seven models and SI-x leaf trends are averaged across 26 models.

The spatial pattern of spring advancement exhibits large variations among models and between the ensemble mean and observations. Both Obs-Berkeley-leaf and Obs-CPC-leaf exhibit relatively large advancement in the Tibetan Plateau, North Russia, and Southern Europe during 1981-2014 (Figure S8), and trends in central and north Asia are statistically significant in Obs-CPC-leaf. This pattern is not present in CMIP6-leaf or any individual model-based SI-x. Moreover, models exhibit significant trends in very few regions (e.g., Eastern NA and Europe in EC-Earth-3-CC and mid-to-high latitude regions in Asia in GFDL-ESM4). The greatest earlier trend in the ensemble mean is in Southern Europe, Eastern US, and the eastern and southern parts of the Rocky Mountains (Figure 3be), but these regions also exhibit large disagreements across models

(Figures 3hj, S8, S9b). When compared to observations, CMIP6-leaf tends to overestimate warming in NA, particularly Western Canada and Eastern US, and underestimate warming in central and north Asia (Figure S10). During 2015-2099, most models exhibit significant earlier spring across the NH (Figures S11b, S12f) and the greatest earlier trend is present in regions along the Pacific coast of NA, in central NA, Europe, and mid-latitude regions of Asia (Figure 3e). Though models mostly agree that spring is starting earlier under the historical and future scenarios (Figures S9b, S11b, S12bdf), large disagreements among models are also present, with ACCESS-CM2, CMCC-ESM2, CNRM-CM6-1, CNRM-CM6-1-HR, EC-Earth3-CC, IPSL-CM6A-LR, TaiESM1, and UKESM1-0-LL experiencing a much larger earlier trend while FGOALS-g3, KIOST-ESM, MRI-ESM2-0, and NESM3 exhibiting a much smaller trend (Figures S8, S10). Compared to the historical period, both the trends and variability of CMIP6-leaf increase in 2015-2099 (Figure 3behj).

Trends of CMIP6-LAI25% vary considerably geographically and across models, but also display an overall earlier spring onset and increasing variability over the NH (Figures 3adgi, S7cd, S9a, S11a, S12ace). During 1950-2014, the mean NH trends of CMIP6-LAI25% is -0.41±0.31 day/decade, ~0.3 day/decade smaller than those indicated by CMIP6-leaf (Figure S7). During 1981-2014, trends of both CMIP6-LAI25% (-0.05±0.29) and Obs-GLASS-LAI25% (-0.01) are close to 0, likely due to the delayed start of spring in areas south of 40°N and Southern Europe (Figures S9a, S11a). The trends change to -0.97±1.06 days/decade during 2015-2099 under the SSP585 scenario, ~1.4 days/decade fewer than trends estimated from CMIP6-leaf (Figure S7). During 1950-2014, the largest trends are present along 60°N in Eurasia and Eastern NA, though trends vary across models in Southern Europe and south of 40°N (Figure 3g). Though CMIP6-LAI25% mean trends are negative (i.e., becomes earlier) in the US, northern Canada, and southern Russia and positive in southern Europe, Obs-GLASS-LAI25% trends in these regions are of smaller amplitude, and sometimes in the opposite direction (Figure S9a). Over the 2015-2099 period, the trend is much stronger in mid-to-high latitude (north of 45°N) and high-altitude regions (Figures 3d, S11a, S12e). In southern Europe and the US, the models diverge in LAI25% responses with large positive trends (delay in spring onset) in CMCC-ESM2, negative trends in EC-Earth3-CC, IPSL-CM6A-LR, and MIROC-ES2L, and contrasting trends in CNRM-ESM2-1.

Although the timing indicated by LAI25% and SI-x leaf vary across models, variabilities and trends derived from the two sets of indicators exhibit relatively good agreement, especially during longer temporal periods and in mid-to-high latitude regions (Figures 3cf, S5c, S9cd, S11cd). During 1981-2014, Obs-GLASS-LAI25% exhibits weaker trends in spring onset timing than Obs-Berkeley-leaf at higher latitudes (north of 50°N) and stronger trends at low latitudes (south of 30°N). This latitudinal pattern is also present in most of the models (except KIOST-ESM) with some variations (Figure S9c). Similar agreement of spring onset trends at mid-to-high latitudes are also present in the ensemble means based on all available models (Figures 3, S13). Although trends of CMIP6-leaf

increase faster than CMIP6-LAI25%, their variabilities are coherent and the difference in their trends is still relatively small and spatially uniform at mid-to-high latitudes (Figures 3, S7, S9, S11, S12, S13). Across the NH, the spread among different indicators is smaller at higher latitudes with the smallest spread present between 55.5°N-84.5°N. However, differences between LAI- and thermal-based indicators increase in the SSP585 scenario across different latitudes, and CMIP6-LAI25% can even be delayed at lower latitudes. At mid-to-high latitudes (north of 40°N except southern Europe), both observations and models exhibit positive and significant correlations between SI-x leaf and LAI25%, except for ACCESS-ESM1-5 in the future scenario and CMCC-ESM2 and KIOST-ESM in some moisture-limited regions (Figures S9d, S11d). Overall, models exhibit an NH mean correlation of 0.47±0.22 during the historical period and 0.43±0.23 under SSP585 between the two sets of indicators.

4 Discussion and conclusion

Our results show good agreement between SI-x leaf calculated from simulated and observed temperatures, but considerable differences are present between model-simulated and observed LAI25% and between LAI25% and SI-x leaf estimated from models. Our results also confirm the later start of the growing season in models presented by previous studies (Park & Jeong, 2021; Peano et al., 2019; Song et al., 2021) and reveal even greater differences in mean DOYs and trends between thermal- and LAI-based indicators projected into the future. Although part of this difference may be due to soil moisture limited plant functional types (PFT) at lower latitudes (Table S2), our results show LAI25% exhibits a less negative trend (i.e., a delayed start of spring) than SI-x leaf at all latitudes, though the indicators are positively correlated (Figures 2, S13). Leaf development in LSMs depends both on spring onset timing and carbon allocation to leaves, so LAI threshold-based indicators reflect the combined influences of biotic and abiotic factors, while SI-x mostly follows environmental impacts. Therefore, SI-x shows the full potential range of temperature-induced spring onset variability while LAI is more restrained by environmental and biotic factors and may therefore be less sensitive to temperature changes. However, the large differences in spring onset timing and trends imply that plant phenology may experience index-related variability and uncertainty as large as or larger than model uncertainty for a given index.

The timing of spring onset has been advancing over the Northern Hemisphere, and the pace is likely to accelerate in the future. Although the start of spring trends in the most recent decade exhibit large uncertainty (Wang et al., 2019), both observations and satellite remote sensing records suggest a long-term advancing trend of spring onset timing (Ault, Schwartz, et al., 2015; Cook et al., 2012; Parmesan & Yohe, 2003; Root et al., 2003; White et al., 2009). We have similarly found earlier spring onset during 1950-2014 in both thermal- and LAI-based indicators which have also been accelerating at mid-to-high latitudes. While thermal-based indicators have been widely adopted to assess future changes in spring onset timing (Allstadt et al., 2015; Zhu et al., 2019),

other environmental factors (e.g., chilling, soil moisture, photoperiod) also influence the start of spring (Flynn & Wolkovich, 2018; Fu et al., 2015; Laube et al., 2014). In addition, changing environments may favor some species and trigger further changes in ecosystem structure and composition (Renner & Zohner, 2018; Wang et al., 2016). Meanwhile, frost risk may also vary as climatic conditions change (Park et al., 2021; Rigby & Porporato, 2008; Zohner et al., 2017), posing additional uncertainty to how natural and managed ecosystems adapt to climate change. Therefore, it is critical to evaluate trends and variability of spring onset in climate models using both meteorological- and vegetation-based indicators and update our predictions as we improve our forecasting approaches.

Agreement between thermal- and LAI-based indicators depends on the phenology schemes adopted in the climate models (Figures S9, S11, Table S2), and the disagreements may further increase the uncertainty in temperature and spring onset projections. LAI- and thermal-based indicators show stronger agreement when phenology is prognostically simulated at higher temporal resolution (i.e., daily or finer). Though temperature dominates spring onset timing of LAI25% at higher latitudes, phenology schemes with only temperature criteria have a higher correlation with SI-x leaf at lower latitudes than phenology schemes with both temperature and soil moisture switches or implicit phenology. As soil moisture and precipitation can be important in triggering spring onset in moisture-limited environments (Dahlin et al., 2015, 2017), the relative importance of temperature may be overestimated in temperature-dominated phenology schemes, though trends of LAI25% still indicate less advancement in spring onset than SI-x leaf in these models. As changes in phenology and growing season length modulate surface temperature (Lorenz et al., 2013; Xu et al., 2020), these disagreements between thermal- and vegetation-based indicators may undermine the credibility of temperature projections and further increase the uncertainty in spring onset timing.

Although models vary considerably in mean onset dates and spring onset trends, the ensemble mean trends are generally good indicators of long-term changes in spring onset timing. Ensemble means of thermal-based indicators agree with observations in both mean dates (Figure S3) and trends (Figures S8, S10). Although CMIP6-LAI25% are later than Obs-GLASS-LAI25% (Figure S5), ensemble mean LAIs (Figure S4) and trends (Figure S9a) exhibit similar magnitude and spatial patterns to GLASS estimates, especially in mid-to-high latitude regions. Ensemble means have proven to be good estimates of meteorological observations (Hagedorn et al., 2005; Palmer et al., 2005) and are widely used for future predictions (Almazroui et al., 2020; Cook et al., 2020). Here we show that the CMIP6 ensemble mean can also be applied to predict spring onset timing. Moreover, because LAI is generally less documented at a high temporal resolution and sometimes prescribed in climate models (e.g. as in CNRM-CM6-1, LAI is prescribed although daily LAI is documented) and LAI- and thermal-based indicators are positively and significantly correlated and largely consistent in their trend differences in mid-to-high latitude regions (Figures S9d, S11d, S12), thermal-based indicators like SI-x can be used to estimate trends and variabili-

ties of LAI seasonal cycles at mid-to-high latitudes.

Plant phenology regulates the terrestrial carbon cycle and land-atmosphere coupling in Earth system models as it influences critical processes such as photosynthesis, respiration, evaporation, and transpiration, yet our results show large disagreements in both the timing and trends of spring onset among models and between models and observations. As LAI-based indicators exhibit later onset and weaker trends than thermal-based indicators, the bias between LAI- and thermal-based spring onset timing may continue to increase in the future, resulting in greater uncertainties in projected spring onset timing. In certain cases, this index-based uncertainty can be larger than inter-model uncertainty for a given index. Indicator models can provide inference on spring onset trends and variability and help isolate the influence of climate factors, but larger uncertainties are present under a warmer climate due to phenology responses to other abiotic and biotic factors. Therefore, studies interested in projected changes in spring phenology should consider variabilities in both meteorological- and vegetation-based indicators, and future work should focus on understanding LAI variability and improving phenology representation in climate models.

Acknowledgments

This work is supported by NSF Macrosystems Biology award (DEB-2017815; DEB-1702551) and NSF Career Award (AGS-1751535). The authors declare no competing interests.

Open Research

The CMIP6 model outputs (maximum and minimum daily temperature, tasmax and tasmin, and leaf area index, lai) are publicly available through the Earth System Grid Federation (ESGF): https://esgf-node.llnl.gov/projects/cmip6/. The extended spring indices and LAI25% DOYs used for this analysis are available in the Figshare repository: https://figshare.com/s/59d3f8ac6c876169f526 and will be made publicly available upon publication of this manuscript.

The code used to calculate the extended spring indices is described in detail in Ault, Zurita-Milla, et al. (2015) and is available at https://github.com/cornell-eas/SI-X.

References

Allstadt, A. J., Vavrus, S. J., Heglund, P. J., Pidgeon, A. M., Thogmartin, W. E., & Radeloff, V. C. (2015). Spring plant phenology and false springs in the conterminous US during the 21st century. *Environmental Research Letters*, *10*(10), 104008. https://doi.org/10.1088/1748-9326/10/10/104008

Almazroui, M., Saeed, S., Saeed, F., Islam, M. N., & Ismail, M. (2020). Projections of precipitation and temperature over the South Asian countries in CMIP6. *Earth Systems and Environment*, *4*(2), 297–320.

Ault, T. R., Schwartz, M. D., Zurita-Milla, R., Weltzin, J. F., & Betancourt, J. L. (2015). Trends and natural variability of spring onset in the coterminous United States as evaluated by a new gridded dataset of spring indices. *Journal of Climate*, *2015*.

Ault, T. R., Zurita-Milla, R., & Schwartz, M. D. (2015). A Matlab© toolbox for calculating spring indices from daily meteorological data. *Computers & Geosciences*, *83*, 46–53. https://doi.org/10.1016/j.cageo.2015.06.015

Benjamini, Y., & Hochberg, Y. (1995). Controlling the False Discovery Rate: A Practical and Powerful Approach to Multiple Testing. *Journal of the Royal Statistical Society. Series B (Methodological)*, *57*(1), 289–300. https://doi.org/10.2307/2346101

Berg, A., Findell, K., Lintner, B., Giannini, A., Seneviratne, S. I., Van Den Hurk, B., Lorenz, R., Pitman, A., Hagemann, S., & Meier, A. (2016). Land–atmosphere feedbacks amplify aridity increase over land under global warming. *Nature Climate Change*, *6*(9), 869–874.

Bi, D., Dix, M., Marsland, S. J., O'Farrell, S., Rashid, H., Uotila, P., Hirst, A. C., Kowalczyk, E., Golebiewski, M., & Sullivan, A. (2013). The ACCESS coupled model: description, control climate and evaluation. *Aust. Meteorol. Oceanogr. J*, *63*(1), 41–64.

Botta, A., Viovy, N., Ciais, P., Friedlingstein, P., & Monfray, P. (2000). A global prognostic scheme of leaf onset using satellite data. *Global Change Biology*, *6*(7), 709–725. https://doi.org/10.1046/j.1365-2486.2000.00362.x

Boucher, O., Servonnat, J., Albright, A. L., Aumont, O., Balkanski, Y., Bastrikov, V., Bekki, S., Bonnet, R., Bony, S., & Bopp, L. (2020). Presentation and evaluation of the IPSL-CM6A-LR climate model. *Journal of Advances in Modeling Earth Systems*, *12*(7), e2019MS002010.

Cao, J., Wang, B., Yang, Y.-M., Ma, L., Li, J., Sun, B., Bao, Y., He, J., Zhou, X., & Wu, L. (2018). The NUIST Earth System Model (NESM) version 3: description and preliminary evaluation. *Geoscientific Model Development*, *11*(7), 2975–2993.

Chuine, I., Cour, P., & Rousseau, D. D. (1998). Fitting models predicting dates of flowering of temperate-zone trees using simulated annealing. *Plant, Cell & Environment*, *21*(5), 455–466.

Cook, B. I., Mankin, J. S., Marvel, K., Williams, A. P., Smerdon, J. E., & Anchukaitis, K. J. (2020). Twenty-first century drought projections in the CMIP6 forcing scenarios. *Earth's Future*, *8*, 6.

Cook, BenjaminI., Wolkovich, ElizabethM., Davies, T. J., Ault, TobyR., Betancourt, JulioL., Allen, JenicaM., Bolmgren, K., Cleland, ElsaE., Crimmins, TheresaM., Kraft, NathanJ. B., Lancaster, LesleyT., Mazer, SusanJ., McCabe, GregoryJ., McGill, BrianJ., Parmesan, C., Pau, S., Regetz, J., Salamin, N., Schwartz, MarkD., & Travers, StevenE. (2012). Sensitivity

of Spring Phenology to Warming Across Temporal and Spatial Climate Gradients in Two Independent Databases. *Ecosystems*, *15*(8), 1283–1294. https://doi.org/10.1007/s10021-012-9584-5

Dahlin, K. M., Fisher, R. A., & Lawrence, P. J. (2015). Environmental drivers of drought deciduous phenology in the Community Land Model. *Biogeosciences*, *12*(16), 5061–5074. https://doi.org/10.5194/bg-12-5061-2015

Dahlin, K. M., Ponte, D. Del, Setlock, E., & Nagelkirk, R. (2017). Global patterns of drought deciduous phenology in semi-arid and savanna-type ecosystems. *Ecography*, *40*(2), 314–323. https://doi.org/10.1111/ecog.02443

Döscher, R., Acosta, M., Alessandri, A., Anthoni, P., Arneth, A., Arsouze, T., Bergmann, T., Bernadello, R., Bousetta, S., & Caron, L.-P. (2021). The EC-earth3 Earth system model for the climate model intercomparison project 6. *Geoscientific Model Development Discussions*, *1*, 2021.

Eyring, V., Bony, S., Meehl, G. A., Senior, C. A., Stevens, B., Stouffer, R. J., & Taylor, K. E. (2016). Overview of the Coupled Model Intercomparison Project Phase 6 (CMIP6) experimental design and organization. *Geoscientific Model Development*, *9*(5), 1937–1958.

Findell, K. L., Gentine, P., Lintner, B. R., & Guillod, B. P. (2015). Data length requirements for observational estimates of land–atmosphere coupling strength. *Journal of Hydrometeorology*, *16*(4), 1615–1635.

Flynn, D. F. B., & Wolkovich, E. M. (2018). Temperature and photoperiod drive spring phenology across all species in a temperate forest community. *New Phytologist*, *219*(4), 1353–1362.

Fu, Y. H., Zhao, H., Piao, S., Peaucelle, M., Peng, S., Zhou, G., Ciais, P., Huang, M., Menzel, A., Peñuelas, J., Song, Y., Vitasse, Y., Zeng, Z., & Janssens, I. A. (2015). Declining global warming effects on the phenology of spring leaf unfolding. *Nature*, *526*(7571), 104–107. https://doi.org/10.1038/nature15402

Gerst, K. L., Crimmins, T. M., Posthumus, E. E., Rosemartin, A. H., & Schwartz, M. D. (2020). How well do the spring indices predict phenological activity across plant species? *International Journal of Biometeorology*, *64*(5), 889–901.

Green, J. K., Konings, A. G., Alemohammad, S. H., Berry, J., Entekhabi, D., Kolassa, J., Lee, J.-E. E., & Gentine, P. (2017). Regionally strong feedbacks between the atmosphere and terrestrial biosphere. *Nature Geoscience*, *10*(6), 410. https://doi.org/10.1038/ngeo2957

Guillevic, P., Koster, R. D., Suarez, M. J., Bounoua, L., Collatz, G. J., Los, S. O., & Mahanama, S. P. P. (2002). Influence of the interannual variability of vegetation on the surface energy balance—A global sensitivity study. *Journal of Hydrometeorology*, *3*(6), 617–629.

Gutjahr, O., Putrasahan, D., Lohmann, K., Jungclaus, J. H., von Storch, J.-S.,

Brüggemann, N., Haak, H., & Stössel, A. (2019). Max planck institute earth system model (MPI-ESM1. 2) for the high-resolution model intercomparison project (HighResMIP). *Geoscientific Model Development*, *12*(7), 3241–3281.

Hagedorn, R., Doblas-Reyes, F. J., & Palmer, T. N. (2005). The rationale behind the success of multi-model ensembles in seasonal forecasting---I. Basic concept. *Tellus A: Dynamic Meteorology and Oceanography*, *57*(3), 219–233.

Hajima, T., Watanabe, M., Yamamoto, A., Tatebe, H., Noguchi, M. A., Abe, M., Ohgaito, R., Ito, A., Yamazaki, D., Okajima, H., Ito, A., Takata, K., Ogochi, K., Watanabe, S., & Kawamiya, M. (2020). Development of the MIROC-ES2L Earth system model and the evaluation of biogeochemical processes and feedbacks. *Geoscientific Model Development*, *13*(5), 2197–2244. https://doi.org/10.5194/GMD-13-2197-2020

Hamdi, R., Degrauwe, D., Duerinckx, A., Cedilnik, J., Costa, V., & Dalkilic T., & T. P. (2014). Evaluating the performance of SURFEXv5 as a new land surface scheme for the ALADINcy36 and ALARO-0 models. *Geoscientific Model Development*, *7*(1), 23–39.

Haxeltine, A., & Prentice, I. C. (1996). BIOME3: An equilibrium terrestrial biosphere model based on ecophysiological constraints, resource availability, and competition among plant functional types. *Global Biogeochemical Cycles*, *10*(4), 693–709.

He, B., Bao, Q., Wang, X., Zhou, L., Wu, X., Liu, Y., Wu, G., Chen, K., He, S., & Hu, W. (2019). CAS FGOALS-f3-L model datasets for CMIP6 historical atmospheric model intercomparison project simulation. *Advances in Atmospheric Sciences*, *36*(8), 771–778.

Held, I. M., Guo, H., Adcroft, A., Dunne, J. P., Horowitz, L. W., Krasting, J., Shevliakova, E., Winton, M., Zhao, M., & Bushuk, M. (2019). Structure and performance of GFDL's CM4. 0 climate model. *Journal of Advances in Modeling Earth Systems*, *11*(11), 3691–3727.

Ito, A., & Oikawa, T. (2002). A simulation model of the carbon cycle in land ecosystems (Sim-CYCLE): a description based on dry-matter production theory and plot-scale validation. *Ecological Modelling*, *151*(2–3), 143–176.

Jolly, W. M., Nemani, R., & Running, S. W. (2005). A generalized, bioclimatic index to predict foliar phenology in response to climate. *Global Change Biology*, *11*(4), 619–632. https://doi.org/10.1111/j.1365-2486.2005.00930.x

Krinner, G., Viovy, N., de Noblet-Ducoudré, N., Ogée, J., Polcher, J., & Friedlingstein P., & P. I. C. (2005). A dynamic global vegetation model for studies of the coupled atmosphere-biosphere system. *Global Biogeochemical Cycles*, *19*, 1.

Laube, J., Sparks, T. H., Estrella, N., Höfler, J., Ankerst, D. P., & Menzel, A. (2014). Chilling outweighs photoperiod in preventing pre-

cocious spring development. *Global Change Biology*, *20*(1), 170–182. https://doi.org/10.1111/gcb.12360

Law, R. M., Ziehn, T., Matear, R. J., Lenton, A., Chamberlain, M. A., Stevens, L. E., Wang, Y.-P., Srbinovsky, J., Bi, D., Yan, H., & Vohralik, P. F. (2017). The carbon cycle in the Australian Community Climate and Earth System Simulator (ACCESS-ESM1) – Part 1: Model description and pre-industrial simulation. *Geoscientific Model Development*, *10*(7), 2567–2590. https://doi.org/10.5194/gmd-10-2567-2017

Lawrence, D. M., Fisher, R. A., Koven, C. D., Oleson, K. W., Swenson, S. C., Bonan, G., Collier, N., Ghimire, B., van Kampenhout, L., & Kennedy, D. (2019). The Community Land Model version 5: Description of new features, benchmarking, and impact of forcing uncertainty. *Journal of Advances in Modeling Earth Systems*.

Lee, J., Kim, J., Sun, M.-A., Kim, B.-H., Moon, H., Sung, H. M., Kim, J., & Byun, Y.-H. (2020). Evaluation of the Korea meteorological administration advanced community earth-system model (K-ACE). *Asia-Pacific Journal of Atmospheric Sciences*, *56*(3), 381–395.

Lee, W. L., Wang, Y. C., Shiu, C. J., Tsai, I. C., Tu, C. Y., Lan, Y. Y., Chen, J. P., Pan, H. L., & Hsu, H. H. (2020). Taiwan Earth System Model Version 1: Description and evaluation of mean state. *Geoscientific Model Development*, *13*(9), 3887–3904. https://doi.org/10.5194/GMD-13-3887-2020

Lehner, F., Deser, C., Maher, N., Marotzke, J., Fischer, E. M., Brunner, L., Knutti, R., & Hawkins, E. (2020). Partitioning climate projection uncertainty with multiple large ensembles and CMIP5/6. *Earth System Dynamics*, *11*(2), 491–508.

Levis, S., & Bonan, G. B. (2004). Simulating springtime temperature patterns in the community atmosphere model coupled to the community land model using prognostic leaf area. *Journal of Climate*, *17*(23), 4531–4540.

Liang, S., Cheng, C., Jia, K., Jiang, B., Liu, Q., Xiao, Z., Yao, Y., Yuan, W., Zhang, X., Zhao, X., & Zhou, J. (2020). The Global LAnd Surface Satellite (GLASS) products suite. *Bulletin of the American Meteorological Society*. https://doi.org/10.1175/BAMS-D-18-0341.1

Liang, S., Zhao, X., Yuan, W., Liu, S., Cheng, X., Xiao, Z., Zhang, X., Liu, Q., Cheng, J., Tang, H., Qu, Y. H., Bo, Y., Qu, Y., Ren, H., Yu, K., & Townshend, J. (2013). A Long-term Global LAnd Surface Satellite (GLASS) Dataset for Environmental Studies. *International Journal of Digital Earth*, *6*, 5–33.

Lorenz, R., Davin, E. L., Lawrence, D. M., Stöckli, R., & Seneviratne, S. I. (2013). How important is vegetation phenology for European climate and heat waves? *Journal of Climate*, *26*(24), 10077–10100.

Lovato, T., Peano, D., Butenschön, M., Materia, S., Iovino, D., Scoccimarro, E., Fogli, P. G., Cherchi, A., Bellucci, A., & Gualdi, S. (2022). CMIP6 Simulations

With the CMCC Earth System Model (CMCC-ESM2). *Journal of Advances in Modeling Earth Systems*, *14*(3), e2021MS002814.

Mahowald, N., Lo, F., Zheng, Y., Harrison, L., Funk, C., Lombardozzi, D., & Goodale, C. (2016). Projections of leaf area index in earth system models. *Earth System Dynamics*, *7*(1), 211–229.

Mauritsen, T., Bader, J., Becker, T., Behrens, J., Bittner, M., Brokopf, R., Brovkin, V., Claussen, M., Crueger, T., Esch, M., Fast, I., Fiedler, S., Fläschner, D., Gayler, V., Giorgetta, M., Goll, D. S., Haak, H., Hagemann, S., Hedemann, C., … Roeckner, E. (2019). Developments in the MPI-M Earth System Model version 1.2 (MPI-ESM1.2) and Its Response to Increasing CO2. *Journal of Advances in Modeling Earth Systems*, *11*(4), 998–1038. https://doi.org/10.1029/2018MS001400

Milly, P. C. D., Malyshev, S. L., Shevliakova, E., Dunne, K. A., Findell, K. L., Gleeson, T., Liang, Z., Phillipps, P., Stouffer, R. J., & Swenson, S. (2014). An enhanced model of land water and energy for global hydrologic and earth-system studies. *Journal of Hydrometeorology*, *15*(5), 1739–1761.

Morisette, J. T., Richardson, A. D., Knapp, A. K., Fisher, J. I., Graham, E. A., Abatzoglou, J., ... & Liang, L. (2009). Tracking the rhythm of the seasons in the face of global change: phenological research in the 21st century. *Frontiers in Ecology and the Environment*, *7*(5), 253-260. https://doi.org/10.1890/070217

Oleson, K. W., Lawrence, D. M., Bonan, G. B., Drewniak, B., Huang, M., Charles, D., Levis, S., Li, F., Riley, W. J., Zachary, M., Swenson, S. C., Thornton, P. E., Bozbiyik, A., Fisher, R., Heald, C. L., Kluzek, E., Lamarque, F., Lawrence, P. J., Leung, L. R., … Sacks, W. (2013). *CLM 4.5 NCAR Technical Note. July.* https://doi.org/10.1007/s11538-011-9690-0

O'Neill, B. C., Tebaldi, C., Van Vuuren, D. P., Eyring, V., Friedlingstein, P., Hurtt, G., Knutti, R., Kriegler, E., Lamarque, J.-F., & Lowe, J. (2016). The scenario model intercomparison project (ScenarioMIP) for CMIP6. *Geoscientific Model Development*, *9*(9), 3461–3482.

Pak, G., Noh, Y., Lee, M.-I., Yeh, S.-W., Kim, D., Kim, S.-Y., Lee, J.-L., Lee, H. J., Hyun, S.-H., & Lee, K.-Y. (2021). Korea institute of ocean science and technology earth system model and its simulation characteristics. *Ocean Science Journal*, *56*(1), 18–45.

Palmer, T. N., Shutts, G. J., Hagedorn, R., Doblas-Reyes, F. J., Jung, T., & Leutbecher, M. (2005). Representing model uncertainty in weather and climate prediction. *Annu. Rev. Earth Planet. Sci.*, *33*, 163–193.

Park, H., & Jeong, S. (2021). Leaf area index in Earth system models: how the key variable of vegetation seasonality works in climate projections. *Environmental Research Letters*, *16*(3), 34027.

Park, I. W., Ramirez-Parada, T., & Mazer, S. J. (2021). Advancing frost dates have reduced frost risk among most North {A}merican angiosperms since 1980.

Global Change Biology, *27*(1), 165–176.

Parmesan, C. (2007). Influences of species, latitudes and methodologies on estimates of phenological response to global warming. *Global Change Biology*, *13*(9), 1860–1872. https://doi.org/10.1111/j.1365-2486.2007.01404.x

Parmesan, C., & Yohe, G. (2003). A globally coherent fingerprint of climate change impacts across natural systems. *Nature*, *421*(6918), 37–42.

Peano, D., Materia, S., Collalti, A., Alessandri, A., Anav, A., Bombelli, A., & Gualdi, S. (2019). Global variability of simulated and observed vegetation growing season. *Journal of Geophysical Research: Biogeosciences*.

Puma, M. J., Koster, R. D., & Cook, B. I. (2013). Phenological versus meteorological controls on land-atmosphere water and carbon fluxes. *Journal of Geophysical Research: Biogeosciences*, *118*(1), 14–29.

Renner, S. S., & Zohner, C. M. (2018). Climate change and phenological mismatch in trophic interactions among plants, insects, and vertebrates. *Annual Review of Ecology, Evolution, and Systematics*, *49*, 165–182.

Richardson, A. D., Anderson, R. S., Arain, M. A., Barr, A. G., Bohrer, G., Chen, G., Chen, J. M., Ciais, P., Davis, K. J., & Desai, A. R. (2012). Terrestrial biosphere models need better representation of vegetation phenology: results from the N orth A merican C arbon P rogram S ite S ynthesis. *Global Change Biology*, *18*(2), 566–584.

Richardson, A. D., Anderson, R. S., Arain, M. A., Barr, A. G., Bohrer, G., Chen, G., ... & Xue, Y. (2012). Terrestrial biosphere models need better representation of vegetation phenology: results from the N orth A merican C arbon P rogram S ite S ynthesis. *Global Change Biology*, *18*(2), 566-584. https://doi.org/10.1111/j.1365-2486.2011.02562.x

Richardson, A. D., Andy Black, T., Ciais, P., Delbart, N., Friedl, M. A., Gobron, N., Hollinger, D. Y., Kutsch, W. L., Longdoz, B., & Luyssaert, S. (2010). Influence of spring and autumn phenological transitions on forest ecosystem productivity. *Philosophical Transactions of the Royal Society B: Biological Sciences*, *365*(1555), 3227–3246.

Richardson, A. D., Hollinger, D. Y., Dail, D. B., Lee, J. T., Munger, J. W., & O'keefe, J. (2009). Influence of spring phenology on seasonal and annual carbon balance in two contrasting New England forests. *Tree Physiology*, *29*(3), 321–331. https://doi.org/10.1093/treephys/tpn040

Richardson, A. D., Keenan, T. F., Migliavacca, M., Ryu, Y., Sonnentag, O., & Toomey, M. (2013). Climate change, phenology, and phenological control of vegetation feedbacks to the climate system. *Agricultural and Forest Meteorology*, *169*, 156–173. https://doi.org/10.1016/j.agrformet.2012.09.012

Rigby, J. R., & Porporato, A. (2008). Spring frost risk in a changing climate. *Geophysical Research Letters*, *35*, 12.

Rohde, R., Muller, R. A., Jacobsen, R., Muller, E., Perlmutter, S., Rosenfeld, A., Wurtele, J., Groom, D., & Wickham, C. (2013). A New Estimate of the Average Earth Surface Land Temperature Spanning 1753 to 2011, Geoinfor Geostat: An Overview 1: 1. *Of*, *7*, 2.

Root, T. L., Price, J. T., Hall, K. R., Schneider, S. H., Rosenzweig, C., & Pounds, J. A. (2003). Fingerprints of global warming on wild animals and plants. *Nature*, *421*(6918), 57–60.

Schwartz, M. D. (1992). Phenology and Springtime Surface-Layer Change. *Monthly Weather Review*, *120*(11), 2570–2578. https://doi.org/10.1175/1520-0493(1992)120<2570:PASSLC>2.0.CO;2

Schwartz, M. D. (1997). Spring Index Models: An approach to connecting Satellite and surface phenology. In *Phenology of Seasonal climates* (Issue 414). pp. 23–38.

Schwartz, M. D., Ahas, R., & Aasa, A. (2006). Onset of spring starting earlier across the Northern Hemisphere. *Global Change Biology*, *12*(2), 343–351. https://doi.org/10.1111/j.1365-2486.2005.01097.x

Schwartz, M. D., Ault, T. R., & Betancourt, J. L. (2013). Spring onset variations and trends in the continental United States: past and regional assessment using temperature-based indices. *International Journal of Climatology*, *33*(13), 2917–2922. https://doi.org/10.1002/joc.3625

Schwartz, M. D., & Marotz, G. A. (1986). An Approach to Examining Regional Atmosphere-Plant Interactions with Phenological Data. *Journal of Biogeography*, *13*(6), 551–560. https://doi.org/10.2307/2844818

Schwartz, M. D., & Reiter, B. E. (2000). Changes in North American spring. *International Journal of Climatology*, *20*(8), 929–932. https://doi.org/10.1002/1097-0088(20000630)20:8<929::aid-joc557>3.0.co;2-5

Séférian, R., Nabat, P., Michou, M., Saint-Martin, D., Voldoire, A., Colin, J., Decharme, B., Delire, C., Berthet, S., & Chevallier, M. (2019). Evaluation of CNRM earth system model, CNRM-ESM2-1: Role of earth system processes in present-day and future climate. *Journal of Advances in Modeling Earth Systems*, *11*(12), 4182–4227.

Seland, Ø., Bentsen, M., Olivié, D., Toniazzo, T., Gjermundsen, A., Graff, L. S., Debernard, J. B., Gupta, A. K., He, Y. C., Kirkeväg, A., Schwinger, J., Tjiputra, J., Schanke Aas, K., Bethke, I., Fan, Y., Griesfeller, J., Grini, A., Guo, C., Ilicak, M., … Schulz, M. (2020). Overview of the Norwegian Earth System Model (NorESM2) and key climate response of CMIP6 DECK, historical, and scenario simulations. *Geoscientific Model Development*, *13*(12), 6165–6200. https://doi.org/10.5194/GMD-13-6165-2020

Sellar, A. A., Jones, C. G., Mulcahy, J. P., Tang, Y., Yool, A., Wiltshire, A., O'Connor, F. M., Stringer, M., Hill, R., Palmieri, J., Woodward, S., de Mora,

L., Kuhlbrodt, T., Rumbold, S. T., Kelley, D. I., Ellis, R., Johnson, C. E., Walton, J., Abraham, N. L., … Zerroukat, M. (2019). UKESM1: Description and Evaluation of the U.K. Earth System Model. *Journal of Advances in Modeling Earth Systems*, *11*(12), 4513–4558. https://doi.org/10.1029/2019MS001739

Semmler, T., Danilov, S., Gierz, P., Goessling, H. F., Hegewald, J., Hinrichs, C., Koldunov, N., Khosravi, N., Mu, L., & Rackow, T. (2020). Simulations for CMIP6 with the AWI climate model AWI-CM-1-1. *Journal of Advances in Modeling Earth Systems*, *12*(9), e2019MS002009.

Sitch, S., Smith, B., Prentice, I. C., Arneth, A., Bondeau, A., Cramer, W., Kaplan, J. O., Levis, S., Lucht, W., Sykes, M. T., & Sitch S., S. B. P. I. C. A. A. B. A. C. W. & V. S. (2003). Evaluation of ecosystem dynamics, plant geography and terrestrial carbon cycling in the LPJ dynamic global vegetation model. *Global Change Biology*, *9*(2), 161–185.

Song, X., Wang, D. Y., Li, F., & Zeng, X. D. (2021). Evaluating the performance of CMIP6 Earth system models in simulating global vegetation structure and distribution. *Advances in Climate Change Research*, *12*(4), 584–595.

Swart, N. C., Cole, J. N. S., Kharin, V. V., Lazare, M., Scinocca, J. F., Gillett, N. P., Anstey, J., Arora, V., Christian, J. R., Hanna, S., Jiao, Y., Lee, W. G., Majaess, F., Saenko, O. A., Seiler, C., Seinen, C., Shao, A., Sigmond, M., Solheim, L., … Winter, B. (2019). The Canadian Earth System Model version 5 (CanESM5.0.3). *Geoscientific Model Development*, *12*(11), 4823–4873. https://doi.org/10.5194/GMD-12-4823-2019

Tatebe, H., Ogura, T., Nitta, T., Komuro, Y., Ogochi, K., Takemura, T., Sudo, K., Sekiguchi, M., Abe, M., & Saito, F. (2019). Description and basic evaluation of simulated mean state, internal variability, and climate sensitivity in MIROC6. *Geoscientific Model Development*, *12*(7), 2727–2765.

Voldoire, A., Saint-Martin, D., Sénési, S., Decharme, B., Alias, A., Chevallier, M., Colin, J., Guérémy, J., Michou, M., & Moine, M. (2019). Evaluation of CMIP6 deck experiments with CNRM-CM6-1. *Journal of Advances in Modeling Earth Systems*, *11*(7), 2177–2213.

Volodin, E. M., Mortikov, E. V., Kostrykin, S. V., Galin, V. Y., Lykossov, V. N., Gritsun, A. S., Diansky, N. A., Gusev, A. V., & Iakovlev, N. G. (2017). Simulation of the present-day climate with the climate model INMCM5. *Climate Dynamics*, *49*(11–12), 3715–3734. https://doi.org/10.1007/S00382-017-3539-7

Volodin, E. M., Mortikov, E. V., Kostrykin, S. V., Galin, V. Y., Lykossov, V. N., Gritsun, A. S., Diansky, N. A., Gusev, A. V., Iakovlev, N. G., Shestakova, A. A., & Emelina, S. V. (2018). Simulation of the modern climate using the INM-CM48 climate model. *Russian Journal of Numerical Analysis and Mathematical Modelling*, *33*(6), 367–374. https://doi.org/10.1515/RNAM-2018-0032

Wang, R., Gamon, J. A., Montgomery, R. A., Townsend, P. A., Zygielbaum, A. I., Bitan, K., Tilman, D., Cavender-Bares, J., & Wang R., G. J. A. M. R. A. T.

P. A. Z. A. I. B. K. & C.-B. J. (2016). Seasonal variation in the NDVI–species richness relationship in a prairie grassland experiment (Cedar Creek). *Remote Sensing*, *8*(2), 128.

Wang, X., Xiao, J., Li, X., Cheng, G., Ma, M., Zhu, G., Altaf Arain, M., Andrew Black, T., & Jassal, R. S. (2019). No trends in spring and autumn phenology during the global warming hiatus. *Nature Communications*, *10*(1), 1–10. https://doi.org/10.1038/s41467-019-10235-8

Wang, Y. P., Law, R. M., & Pak, B. (2010). A global model of carbon, nitrogen and phosphorus cycles for the terrestrial biosphere. *Biogeosciences*, *7*(7), 2261–2282.

White, M. A., Beurs, K. M. De, Didan, K., Inouye, D. W., Richardson, A. D., Jensen, O. P., O'keefe, J., Zhang, G., Nemani, R. R., Leeuwen, W. J. D. Van, Brown, J. F., Wit, A. De, Schaepman, M., Lin, X., Dettinger, M., Bailey, A. S., Kimball, J., Schwartz, M. D., Baldocchi, D. D., … Lauenroth, W. K. (2009). Intercomparison, interpretation, and assessment of spring phenology in North America estimated from remote sensing for 1982–2006. *Global Change Biology*, *15*(10), 2335–2359. https://doi.org/10.1111/j.1365-2486.2009. 01910.x.

White, M. A., Thornton, P. E., & Running, S. W. (1997). A continental phenology model for monitoring vegetation responses to interannual climatic variability. *Global Biogeochemical Cycles*, *11*(2), 217–234. https://doi.org/10.1029/97GB00330

Wu, T., Lu, Y., Fang, Y., Xin, X., Li, L., Li, W., Jie, W., Zhang, J., Liu, Y., Zhang, L., Zhang, F., Zhang, Y., Wu, F., Li, J., Chu, M., Wang, Z., Shi, X., Liu, X., Wei, M., … Liu, X. (2019). The Beijing Climate Center Climate System Model (BCC-CSM): The main progress from CMIP5 to CMIP6. *Geoscientific Model Development*, *12*(4), 1573–1600. https://doi.org/10.5194/GMD-12-1573-2019

Xu, X., Riley, W. J., Koven, C. D., Jia, G., & Zhang, X. (2020). Earlier leaf-out warms air in the north. *Nature Climate Change*. https://doi.org/10.1038/s41558-020-0713-4

Yukimoto, S., Kawai, H., Koshiro, T., Oshima, N., Yoshida, K., Urakawa, S., Tsujino, H., Deushi, M., Tanaka, T., Hosaka, M., Yabu, S., Yoshimura, H., Shindo, E., Mizuta, R., Obata, A., Adachi, Y., & Ishii, M. (2019). The meteorological research institute Earth system model version 2.0, MRI-ESM2.0: Description and basic evaluation of the physical component. *Journal of the Meteorological Society of Japan*, *97*(5), 931–965. https://doi.org/10.2151/JMSJ.2019-051

Zhu, L., Meng, J., Li, F., & You, N. (2019). Predicting the patterns of change in spring onset and false springs in China during the twenty-first century. *International Journal of Biometeorology*, *63*(5), 591–606.

Zohner, C. M., Mo, L., Renner, S. S., Svenning, J. C., Vitasse, Y., Benito, B.

M., ... & Crowther, T. W. (2020). Late-spring frost risk between 1959 and 2017 decreased in North America but increased in Europe and Asia. *Proceedings of the National Academy of Sciences*, *117*(22), 12192-12200.